INVESTIGATION OF ABNORMAL BEHAVIOR OF LIGHT INDUCED DEGRADATION (LID) IN COST-EFFECTIVE INDUSTRIAL ALUMINUM BACK SURFACE FIELD (Al-BSF) SILICON SOLAR CELLS

by

Yu-Chen Hsu

A thesis submitted to the faculty of
The University of North Carolina at Charlotte
in partial fulfillment of the requirements
for the degree of Master of Science in
Electrical Engineering

Charlotte

2017

Approved by:

Prof. Abasifreke Ebong

Prof. Yong Zhang

Prof. M. Yasin Akhtar Raja

ABSTRACT

YU-CHEN HSU. Investigation of abnormal behavior of light induced degradation (LID) in cost-effective industrial aluminum back surface field (Al-BSF) silicon solar cells. (Under the direction of DR. ABASIFREKE EBONG)

In this research, the p-type boron-doped (B-doped) Czochralski (Cz) mono crystalline silicon (c-Si) Al-BSF solar cell was studied because of its large market share, high efficiency potential (~20%) and cost-effectiveness. The main problem of the p-type B-doped Cz silicon is the unstable efficiency due to the light induced degradation (LID).

In order to resolve this unstable-efficiency problem, this thesis work investigated the causes and mitigation of LID. The major cause of LID is the formation of boron-oxygen defect in the silicon bandgap under irradiation. The reduced lifetime due to recombination in the bandgap can be recovered by two methods including (i) ~200˚C low temperature anneal or (ii) rapid thermal anneal at 630-850°C. LID can be prevented with alternative base-doping such as Ga, P, or the use of high base resistivity in boron doped Si. However, the latter is still in the research stage while the majority of the commercial solar cell is boron doped with resistivity ranging from 0.5-2 Ω-cm. Therefore, there is a greater need to fully understand how to get rid of the LID in the finished cells.

This thesis work focuses on regeneration of cells after the contact co-firing step or/and degraded state. Regeneration is a stable recovery, which encompasses degradation, recovery and stability. Two experimental set ups were conducted by controlling (i) the carrier injection (~1 sun), (ii) the temperatures (70-100°C), and (iii) time (> 24 hours). The cells went through degradation, recovery and stabilization under irradiation.

The recombination centers constituted of the boron-oxygen related defect are passivated by the effusion of hydrogen existing in the anti-reflection coating (ARC) of a solar cell. During the contact co-firing process after the screen printing, hydrogen enable to diffuse from ARC into the bulk. If the cooling rate is fast in the co-firing, then the future LID degradation is less because some of the hydrogen is retained at the recombination sites.

Regeneration is based on hydrogenation. First, the hydrogen from ARC diffuses into the bulk during the contact co-firing. Subsequently, through the regeneration process, the hydrogen in the bulk transfers to atomic and mobile hydrogen at excited states, and finally passivates defect into equilibrium. The regeneration process requires simultaneous (i) the carrier injection (> 0.1 suns), (ii) elevated temperatures (65-400°C) and (iii) the sufficient time.

Hydrogenation through regeneration process results in stable solar cells. In comparison between the results in this thesis and previous studies in literature, it can be concluded that the faster regeneration rate primarily depends on the temperatures. The higher the temperature in a proper range, the shorter the time required for regeneration.

DEDICATION

This work is dedicated to

God and Buddha for endless Love and Blessing

my beloved parents, Wen-Hsien Hsu and Tzu-Yu Wang,

for fostering and educating me with infinite love and support

my two older sisters, Lisa Hsu and Trista Hsu,

for their benevolent sacrifice, patience and backup

my closed cousins, Che-Ming Hsu, Ming-I Hsu, Hsien-Chang Hsu,

for their kind assistance and inspiring encouragement

ACKNOWLEDGEMENTS

This thesis was not accomplished on my own but with God, Buddha, my professors, team members, and boyfriend. Without their support and assistance, I would have been unable to build this milestone in my life.

First of all, I would like to express my extreme gratitude to God/Buddha. God/Buddha has blessed me to choose the United Sates and UNC Charlotte to develop my graduate study. During my study, God/Buddha has guided me to learn from outstanding people. God/Buddha has brought me to encounter kind-hearted people and to receive immediate help from them. God/Buddha has inspired me to build my confidence and to fight difficulties. Without the backup from God/Buddha, I would not be who I am today.

I am deeply indebted to my research advisor, Professor Abasifreke Ebong, who is like my father in the U.S. Prof. Ebong has spent time teaching me how to write and speak in a technical way. He has patiently discussed my research and trained me to think logically and independently. He has provided me with research resources and opportunities to overcome my limits, expand my knowledge, and improve my abilities. Prof. Ebong has contributed the most to my thesis. Without his motivation and promotion, I would not have made it this far in my master's degree.

I am extremely grateful to my school family and team members, Stephanie LaChair, Veysel Unsur, Ahrar A. Chowdhury, Pankaj Bhowmik, Mayangi Mvutu, and Nian Chen. Prof. Ebong is like my father while Stephanie is like my mother. She is so brilliant and effectively helped me to deal with different problems. She has an ability to make students more attached to our department. Veysel and Ahrar are good partners and Samaritans in my research. They have taught me how to conduct screen printing and RTP by IR belt furnace. During our discussion about papers, experiments and results, they have helped me build PV foundations and contributed great ideas to this work. They contribution to my work is truly respectable in my mind.

Additionally, Pankaj wisely suggested how to complete effective and successful research and presentation. He kindly taught and assisted me to finish projects of smart-grid solar systems. Mayangi (May) and I studied PV and grew up together when we participated in the lab at the same time. He was willing to share what he learned and did with me. His MS thesis and defense slides helped my progress of writing thesis. Although he graduated last year, he is still concerned about my research and encourages me. Nian is my research model because of his professionalism. He provided me with useful suggestions and his PhD thesis as a reference. His excellent work functioned as a guide book that taught me the right attitude to doing research and writing a thesis.

I really appreciate that Prof. Yong Zhang and Prof. Yasin Raja were willing to be my defense committee members and gave me constructive advice. Prof. Yong Zhang particularly debugged the blind spot in my LID research with his strong physics background. Without his valuable ideas, I would not have completed this work with such polish.

I would like to give special thanks to Ms. Constance M. Fessler, Dr. Lisa Russell-Pinsoin, and Dr. Smith Stuart. They demonstrated their responsibility in courses, strongly influencing me to behave in a responsible way. Ms. Fessler has improved my communication skills of speaking and presentation. Her helpful lecture certainly will benefit me to adapt to my career. Dr. Lisa taught me professional writing for research. She always encourages her students while observing the talent of each student. Her encouragement inspires me a lot in my graduate life. Dr. Smith with enthusiasm for his research arouses my passion for my solar study. He is patient and willing to discuss questions with students. I have learned how to do a good job with a passion and willingness from him. He also provide me valuable learning opportunities, expanding my knowledge of nanofabrication.

Last but not least, I am really thankful to have Babacar Diouf, my boyfriend, as well as Jason Ho and Chia-Hua Huang, my former teachers in Taiwan. Their trust and belief have inspired me to conquer the struggling in my research. Their constant encouragement and support have motivated me to work harder and better than my best.

TABLE OF CONTENTS

LIST OF TABLES

LIST OF FIGURES

LIST OF SYMBOLS/ABBREVIATIONS

3-BB	3-busbar
Ag	silver
Al	aluminum
ARC	antireflection coating
BSF	back surface field
c-Si	crystalline silicon
Cz	Czochralski
E_i	intrinsic Fermi level
E_c	conduction band
E_v	valence band
FF	fill factor
FZ	float-zone
ipm	inch per minute
IR heat lamp	infrared heat lamp
J_L	light-generated current density
J_{o1}	saturation current density
J_{o2}	junction reverse saturation current density
J_{ob}	base saturation current density
J_{oe}	emitter saturation current density
J_{sc}	short-circuit current density
LID	light-induced degradation

LPCVD	low pressure chemical vapor deposition
MCz	Magnetic Czochralski
N_t	metastable defect concentration
N_t	trap density
N_t	defect concentration
N_t*	normalized trap density
N_t*	normalized defect concentration
N_{res}	residential defect concentration
SRH theory	Shockley-Real-Hall theory
σ	capture cross section
σ_{res}	the residential capture cross section
PECVD	plasma-enhanced chemical vapor deposition
QSSPC measurement	quasi-steady-state photoconductance measurement
R_s	series resistance
SiN_x	silicon nitride
SiO_2	silicon dioxide
τ_{SRH}	Shockley-Real-Hall lifetime
τ_o	initial bulk lifetime
τ_d	final degraded lifetime
τ_b	bulk lifetime
τ_{eff}	effective lifetime
TDLS	temperature-dependent lifetime spectroscopy
ν_{th}	thermal velocity

CHAPTER 1: FUNDAMENTAL PRINCIPLE OF SOLAR CELLS

1.1 Introduction

Photovoltaics (PV) effect was first observed in 1839 by Becquerel [1]. Since then it has been extensively studied and commercialized in 1955 [2] in order to resolve the global energy crisis. It is environmentally friendly compared to conventional energy sources, which pollutes. Photovoltaics has been widely used in the residential and industrial market in recent years. According to Renewables 2016 Global Status Report [3], Fig. 1.1, solar energy has grown much faster than other renewable energy, such as wind power, geothermal power and hydropower since 2010. It is also estimated that solar energy created ~2.8 million jobs among 8.1 million jobs in renewable-energy between 2010 and 2015 [3]. Thus, solar energy provided over 30% job opportunities of the renewable energy as shown in Fig. 1.1 [3]. Therefore, solar energy not only contributes to the environmental friendliness but to the economic growth.

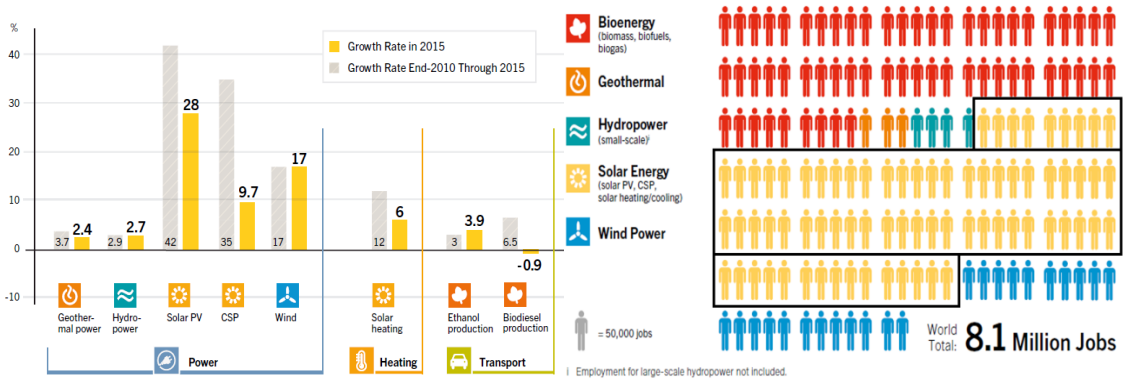

Fig 1.1 (Left): Average annual growth rates of renewable energy capacity and biofuels production, end-2010 to end-2015 [3]. (Right): Estimated direct and indirect jobs in renewable energy worldwide; data are principally for 2014- 2015 by industry [3].

1.2 Solar Cell Structure and Operation Principle

1.2.1 Al-BSF Solar Cell Structure

The Al-BSF structure is the most commercialized solar cell structure. The back surface field, which is the p^+/p region create by the Al-alloyed silicon functions as a filed-effect passivation layer. The Al-doped p^+/p creates a barrier to block the minority carriers flow to the rear surface, reducing surface recombination (Fig. 1.2). Generally, mono- and multi- c-Si solar cells use p-type boron-doped substrate. Fig. 1.3 shows a typical p-type Al-BSF cell: (1) the front contact screen-printed with silver (Ag) paste, (2) the antireflection coating (ARC) to reduce reflectance and allow more photons to be absorbed, and passivates the surface as well, (3) the emitter formed by diffusing phosphorous (P) into the p-type substrate, (4) the p-type base doped with boron (B), (5) the BSF layer for reducing the recombination loss, and (6) the rear contact screen-printed with Aluminum (Al) paste.

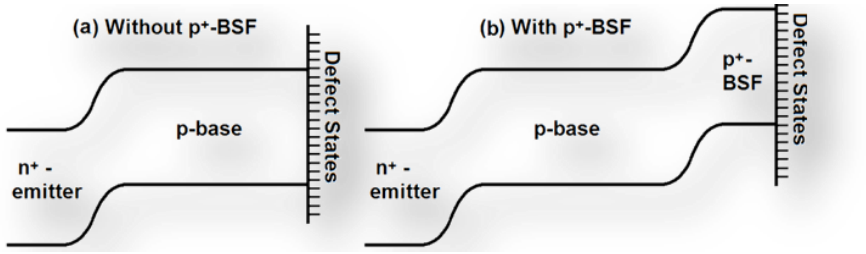

Fig 1.2: Band diagrams illustrating band-bending caused by Al BSF [4].

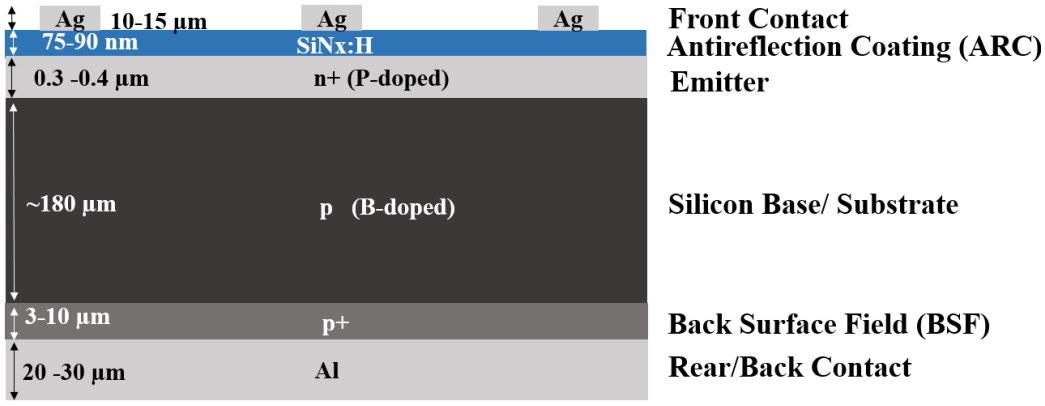

Fig 1.3: Basic architecture structure of a solar cell and general thickness of each layer.

1.2.2 Photovoltaic Effect

A solar cell is a semiconductor device, which converts sunlight into electricity without any polluting byproducts. On the basis of the photovoltaic effect, if incident photon-energy is higher than the band gap (*Eg*) of the semiconductor, the absorbed photons will stimulate the electrons from the valence band (E_v) into the conduction band (E_c), generating electron-hole pairs, as shown in Fig. 1.4.

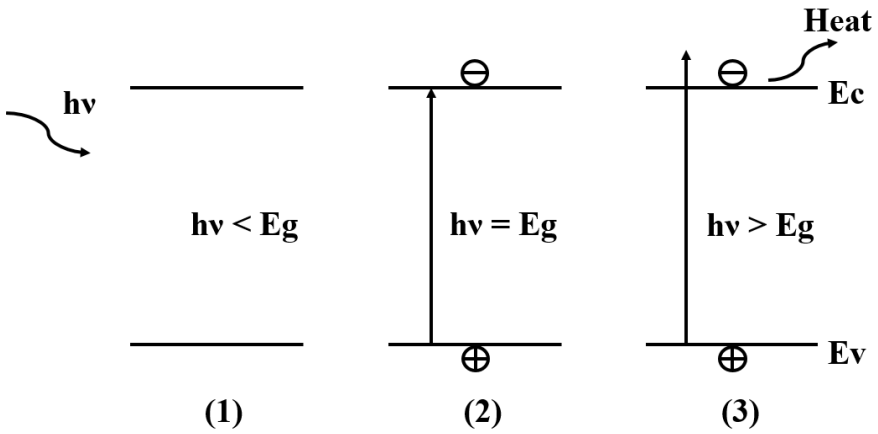

Fig 1.4: Energy diagram of a photon entering the semiconductor.

(1) *hv* < *Eg*: photon fails to generate an electron-hole pair.
(2) *hv* = *Eg*: photon accurately generates an electron-hole pair.
(3) *hv* > *Eg*: photon generates an electron-hole pair; transfers the rest energy into heat.

1.2.3 The p-n Junction Diode in Semiconductor

A solar cell is considered as a p-n junction diode (Fig 1.5). Under illumination, the electrons as minority carriers in the p type region are forced by the electric field and drift across the depletion region toward the n-type area becoming majority carriers (Fig. 1.6). When the front and rear electrodes connect with an initial bias, forming a circuit, a photocurrent (I_L) is generated.

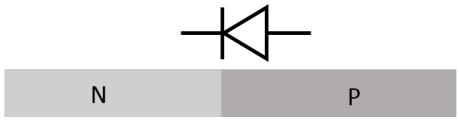

Fig 1.5: Correlation between a p-n junction and an ideal diode.

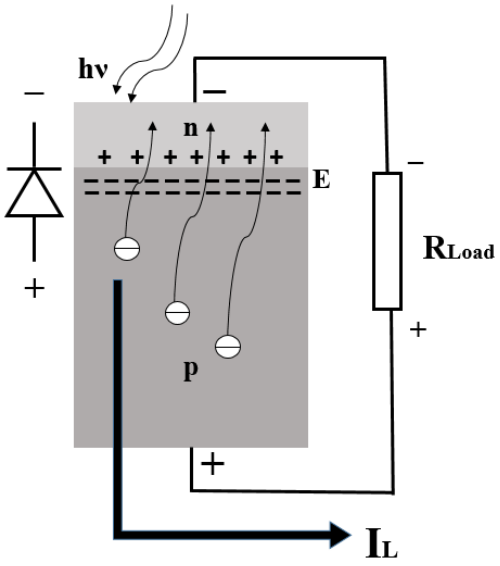

Fig 1.6: Under illumination, the reduced potential barrier (E) enables the minority carrier electrons in the p-type region to drift into n-type region as a major carrier, generating a photocurrent (I_L).

1.3 Electrical Output Parameters of a Solar Cell

1.3.1 Equivalent Circuit

Under ideal condition, the equivalent circuit of a solar cell consists of only one diode, as illustrated in Fig 1.7. Generally, the total current density, J (A/cm^2), considers photocurrent density and ideal diode current density as written Eq. 1.1 and Eq. 1.2.

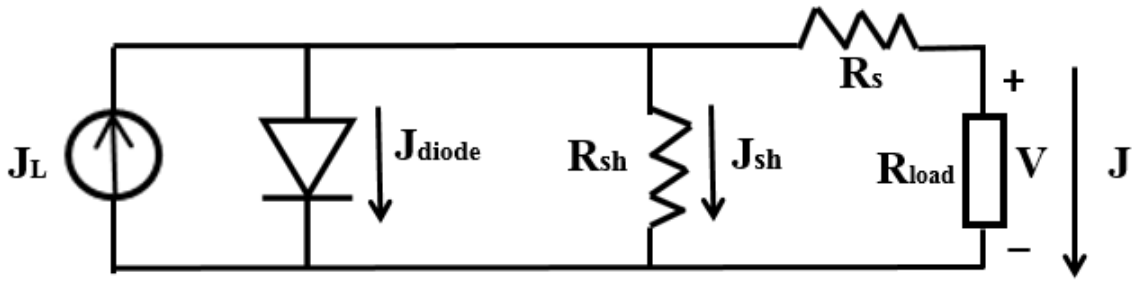

Fig 1.7: Equivalent circuit of ideal one-diode model of a solar cell under illumination.

$$J = J_L - J_{diode} \qquad \text{(Eq. 1.1)}$$

$$J = J_L - J_0\left(\exp\frac{qV}{nkT} - 1\right) \qquad \text{(Eq. 1.2)}$$

where n is ideality factor; $n = 1$ for an ideal diode while $n > 1$ for a non-ideal diode; J_0 is a reverse-biased saturation current density, R_{load} is a load resistance, J_{total} is output current density and V is output voltage. In this ideal condition, the shunt resistance (R_{sh}) is assumed very large leading J_{sh} almost to zero while the series resistance (R_s) is assumed as zero without any voltage loss. R_s includes the resistance of busbars, fingers, front contacts, emitter, bulk, and backside.

However, the p-n junction diode is non-ideal under illumination because of the recombination current loss. As illustrated in Fig. 1.8, Eq. 1.3, and Eq. 1.4, under illumination, the total current density (J) consists of photocurrent density (J_L), diode current density (J_{01}), recombination current density (J_{02}), and a shunt current density (J_{sh}).

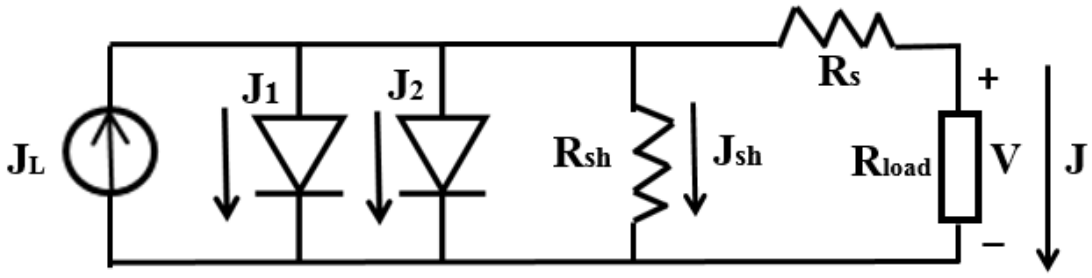

Fig 1.8: The equivalent circuit of non-ideal two diode model under illumination.

$$J = J_L - (J_1 + J_2 + J_{sh}) \qquad \text{(Eq. 1.3)}$$

$$J = J_L - \left\{ J_{01}\left(\exp\frac{q(V + JR_s)}{n_1 kT} - 1 \right) + J_{02}\left(\exp\frac{q(V + JR_s)}{n_2 kT} - 1 \right) + \frac{V + JR_s}{R_{sh}} \right\} \qquad \text{(Eq. 1.4)}$$

where J_{01} is a reverse-biased saturation current density, J_{02} is a recombination current density, n_1 and n_2 are the ideality factor. Similar to the ideal condition, R_s is expected to be minimized and R_{sh} to be maximized through the cell design and manufacturing. Most of all, J_{o2} as a recombination loss has to be reduced in order to improve the efficiency. Recombination loss can occur at the surface/emitter, metal contacts, and bulk (Radiative recombination, Auger recombination, and Shockley-Real-Hall recombination). In this work, Shockley-Real-Hall recombination is being focused on and will be discussed in Chapter 2.

1.3.2 Electrical Output Parameters

In the analysis of the performance of a solar cell, the circuit is considered in two conditions. First, when a series resistance (R_s) and a load resistance (R_{load}) are zero, the maximum current flowing in the circuit is a short-circuit current density (J_{sc}) (Eq. 1.5).

$$J_{sc} = J_L - \left\{ J_{01}\left(\exp\frac{qV}{n_1 kT} - 1 \right) + J_{02}\left(\exp\frac{qV}{n_2 kT} - 1 \right) \right\} \qquad \text{(Eq. 1.5)}$$

Secondly, assuming R_{load} and R_s to be infinity, the total current is zero while J_L is considered as J_0 or J_{diode} (Eq. 1.6). In this condition, the terminal voltage is maximum, called an open-circuit voltage (V_{oc}) (Eq. 1.7). In the results of this work, V_{oc} values were considered to evaluate the recombination in the bulk.

$$J = J_L - J_0\left(\exp\frac{qV_{oc}}{nkT} - 1 \right) = 0 \qquad \text{(Eq. 1.6)}$$

$$V_{oc} = \frac{nkT}{q}\ln\left(\frac{J_L}{J_0} + 1 \right) = \frac{nkT}{q}\ln\left(\frac{J_L}{J_{oe} + J_{ob}} + 1 \right) \qquad \text{(Eq. 1.7)}$$

where J_{oe} is emitter saturation current density and J_{ob} is base saturation current density.

Assuming $J_L = J_{sc}$, the general function of V_{oc} is as given in Eq. 1.8. The reverse saturation current (J_{o1}) is composed of emitter saturation current density (J_{oe}) (Eq. 1.9) and base saturation current density (J_{ob}) (Eq. 1.10), as written in Eq. 1.11 [60].

$$V_{oc} = \frac{nkT}{q} \ln\left(\frac{J_{sc}}{J_{oe} + J_{ob}} + 1 \right) \quad \text{(Eq. 1.8)}$$

$$J_{oe} = F_m J_{oem} + (1 - F_m) J_{oeSiN} \quad \text{(Eq. 1.9)}$$

$$J_{ob} = \frac{q n_i^2}{N_A} \frac{D}{L_{eff}} \quad \text{(Eq. 1.10)}$$

$$J_{o1} = J_{oe} + J_{ob} \quad \text{(Eq. 1.11)}$$

where F_m is the metal grid area coverage faction, J_{oem} is the emitter saturation current density underneath the metal grid, and J_{oeSiN} is the emitter saturation current density of the nitride passivated emitter between grid lines. q is the elementary charge, n_i is the intrinsic carrier density, N_A is the acceptor carrier density, D is the diffusivity of minority, and L_{eff} is the effective minority diffusion length.

The conversion efficiency (η) is defined as the ratio of output power to input power, as shown is Eq. 1.12. The maximum output power is the product of the maximum voltage (V_m) and the maximum current (I_m), where V_m can be determined by trial and error. Then, I_m can be determined when $V = V_m$, as illustrated in Figure 1.9.

$$\eta = \frac{P_{out}}{P_{in}} = \frac{P_{\max}}{P_{in}} = \frac{V_m I_m}{P_{in}} \qquad \text{(Eq. 1.12)}$$

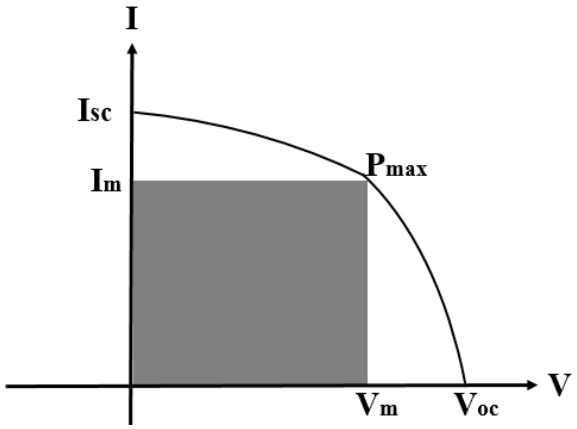

Fig 1.9: I-V characteristic curve.

Fill factor (*FF*) is defined as a ratio of maximum power to total power under I-V curve (Fig. 1.9 and Eq. 1.13) and influenced by the contact quality – *FF* (R_s, R_{sh}, n, J_{02}) [4]. As determined in Eq. 1.14, *FF* is a vital parameter to evaluate the efficiency of a solar cell. The general value of *FF* is between 0.7 and 0.85.

$$FF = \frac{P_{\max}}{V_{oc} I_{sc}} = \frac{V_m I_m}{V_{oc} I_{sc}} \qquad \text{(Eq. 1.13)}$$

$$\eta = \frac{V_m I_m}{P_{in}} = \frac{V_{oc} I_{sc} FF}{P_{in}} \qquad \text{(Eq. 1.14)}$$

1.4 Commercial Status of the c-Si Al-BSF Solar Cell

According to 2014 solar technology report [5], 91% of the solar module around the world is manufactured with silicon. In general, silicon solar cells are fabricated on both mono- and multi- crystalline substrates. Mono crystalline (c-Si) generally exhibits high minority carrier lifetime whereas the multi c-Si because of several grain and grain boundaries exhibits lower minority carrier lifetime. As shown in Fig. 1.10, the Al-BSF cells made on mono and multi Si, account for ~50% of the solar module market in 2014, the most commercialized structure comparing to other technologies [5].

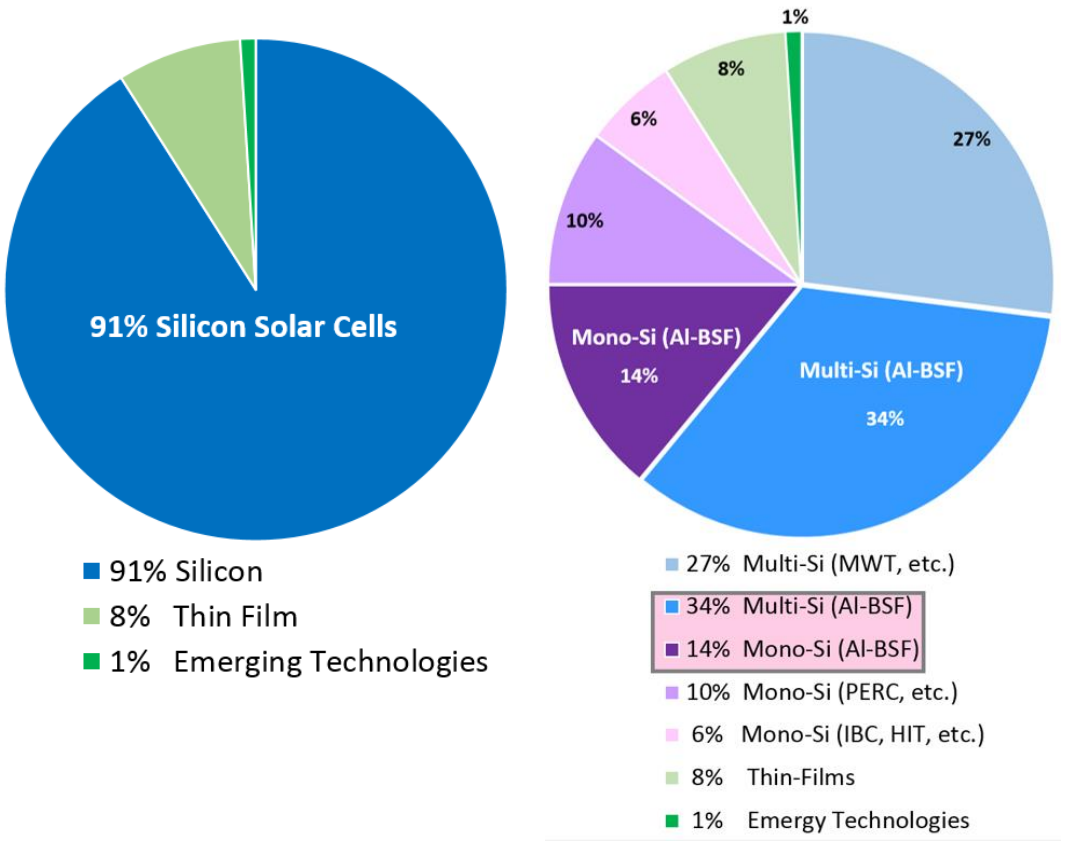

Fig 1.10: PV module production share in 2014 by technology (MW) [5].
(MWT: metal wrap through cell) (PERC: passive emitter and rear cell)
(IBC: interdigitated back contact cell) (HIT: heterojunction with intrinsic thin-layer)

1.5 Motivation and Problem Statement

Al-BSF c-Si solar cell is the most commercialized solar module accounting for ~50% of the market share. However, only ~14% of these Al-BSF Si modules are mono-crystalline. Although the market share of the mono is lower than the multi c-Si Al-BSF structure, the mono c-Si is chosen in this work because of its higher efficiency potential (Table 1.1) and ease of reproducibility. In spite of the performance advantages, the efficiency of the p-type B-doped mono c-Si solar cells is unstable under sunlight, due to the light-induced degradation (LID), as shown in Table 1.2. This phenomenon is mainly observed with cells fabricated on boron doped Cz Si with high oxygen concentration. Therefore, in order to produce stable performing solar cells, this thesis work investigated the causes and mitigation of LID.

Table 1.1: General output values of Al-BSF mono c-Si solar cells.

V_{oc} *(mV)*	*Jsc (mA/cm^2)*	*FF (%)*	*η (%)*
620~650	35~39	76~80	16~20

Table 1.2: Analysis of the strengths and weakness of Al-BSF mono c-Si.

	Advantage	Disadvantage
Commercial Mark Share	14%	
Reliability or Longevity	+25 years [5]	
Efficiency	~20 %	Unstable (LID)
Manufacturing Cost	Cheaper	

CHAPTER 2: UNDERSTANDING THE CAUSES OF LID

2.1 LID Phenomenon

In 1972, Crabb discovered solar cells degraded severely under irradiation [12]. 1973, Fisher and Pschunder observed that the minority carrier lifetime decayed with the illumination time by up to 10% [7]. LID phenomenon occurred when the p-type B-doped Cz or crucible-growth (CG) Si solar cells with rich oxygen was under illumination at room temperatures [7]. However, the causes of LID was not identified.

In 1979, Weizer et al. reported that I_{sc} of the n^+/p cells degraded when a forward bias of $>0.5\ V$ was applied in the dark for 45 sec. They concluded that excess carriers (Δn) could decay p-type cells; which was called carrier injection degradation or CID [8]. Therefore, the excess minority carriers can be caused by illumination or forward bias. Since the bulk lifetime (τ_b) strongly depends on the injection level, the general definition of the bulk lifetime is the quotient of the excess carrier concentration (Δn) and net recombination rate (U), as written in Eq. 2.1 [37]. The defect formation in LID can be accelerated by higher light intensity of the carrier injection [9], such as laser [62].

$$\tau = \frac{\Delta n}{U} \qquad \text{(Eq. 2.1)}$$

2.2 Causes of LLD

2.2.1 Shockley-Real-Hall Recombination

In 1952, Shockley, Real [10] and Hall [11] showed that electron-hole pairs recombine through the mechanism of trapping occurring within the bandgap, called Shockley-Real-Hall (SRH) theory of recombination (Fig 2.1). The trap or defect at forbidden energy states could capture both electrons and holes with approximately equal probability, acting as the recombination center [31]. SRH recombination is considered responsible for LID degradation.

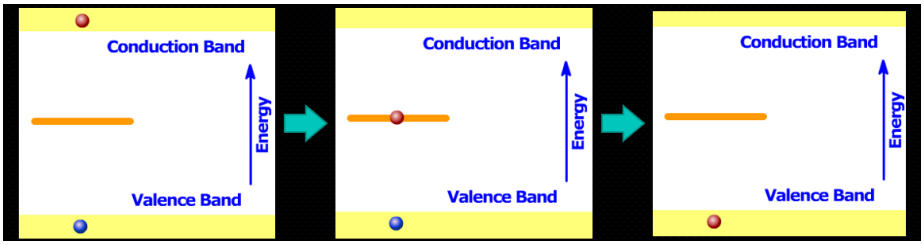

Fig 2.1: Shockley-Real-Hall recombination takes place at the trap in the bandgap [13].

According to the SRH theory, in 1999, Schmidt and Cuevas proposed that, by injection-dependent lifetime spectroscopy (IDLS), the shallow recombination center (E_t) was simulated at the energy level $(E_v + 0.15)\ eV$ or $(E_c - 0.15)\ eV$ within the bandgap under illumination [14]. Furthermore, the deep recombination center (E_t) was activated between $(E_v + 0.35 \text{ and } E_c - 0.45)\ eV$, relatively close to the intrinsic Fermi level (E_i) of silicon $(E_t - E_i < 0.2\ eV)$ [14]. In 2003, Rein and Glunz determined the metastable defect energy level $E_t = E_c - 0.4\ eV$ by higher accuracy measurement with temperature-dependent lifetime spectroscopy (TDLS) [15]

SRH lifetime (τ_{SRH}) was demonstrated (Eq. 2.1) by Schmidt and Cuevas through contactless quasi-steady-state photoconductance (QSSPC) measurement [14, 15]. They assumed that (i) total defect is activated after illumination, (ii) all defect is deactivated after 200 °C annealing and (iii) the illumination did not induce other recombination within the Cz wafer and SiN_x passivation coating, such as Auger recombination and surface recombination [14, 15]. Based on the same assumption, the trap density (N_t) caused by illumination is directly proportional to ($l/\tau_d - l/\tau_o$) as presented in Eq. 2.3, 2.4 and 2.5 [16, 17, 18, 24, 59].

$$\tau_{SRH} = \left(\frac{1}{\tau_o} - \frac{1}{\tau_d}\right)^{-1} \qquad \text{(Eq. 2.2)}$$

$$N_t^* \equiv \frac{1}{\tau_d} - \frac{1}{\tau_0} = \left(\frac{1}{\tau_{\text{meta}}} + \frac{1}{\tau_{res}}\right) - \frac{1}{\tau_{\text{res}}} \qquad \text{(Eq. 2.3)}$$

$$N_t^* = \left(\frac{1}{\tau_{\text{meta}}} + \frac{1}{\tau_{res}}\right) - \frac{1}{\tau_{\text{res}}} = \left(\nu_{th}\sigma\, N_t + \nu_{th}\sigma_{res}N_{res}\right) - \nu_{th}\sigma_{res}N_{res} \qquad \text{(Eq. 2.4)}$$

$$N_t^* = \frac{1}{\tau_{\text{meta}}} = \nu_{th}\sigma\, N_t \qquad \text{(Eq. 2.5)}$$

where τ_d is the final stable effective lifetime after complete light degradation and τ_o is the effective carrier lifetime measured right after the low temperature 200°C annealing. ν_{th} is the thermal velocity, σ is the capture cross section, σ_{res} is the residential capture cross section, N_t is the concentration of the metastable defect, and N_{res} is the residential defect concentration.

2.2.2 BO Complex

In 1973, when Fischer and Pschunder observed the B-doped Cz silicon wafer degradation under illumination, they also found a complete recovery from LID by ~200°C annealing [7]. Since then, several studies have been undertaken to understand the causes of LID and the degradation/recovery cycle in B-doped Cz silicon solar cells.

In 1997, Schmidt et al. presented a model of the B_iO_i pair contribution to the unstable carrier lifetimes in B-doped Cz silicon under illumination, predicting that the defect quantity should increase linearly with the product of boron [N_B] and oxygen concentration [Oi] [16]. However, in 1998, Glunz et al. found that the lifetime degraded with nearly rising [N_B], but with a strongly super linear increasing [Oi], approximately to the power of 5, suggesting the defect complex difference from the B_iO_i model [17]. In 1999, Schmidt and Cuevas analyzed that the energy level of the LID recombination center differed from the B_iO_i pair by injection-level-dependent lifetime spectroscopy [14]. They proposed a defect structure of one substitutional boron (B_s) and several oxygen atoms [14].

In 2004, Schmidt and Bothe presented the metastable B_s-O_{2i} complex formed when fast-diffusing oxygen dimer (O_{2i}) were captured by B_s [20]. This B_s-O_{2i} complex model was based on the dependencies of measured linear N_t*([B_s]) and quadratic N_t*([O_i]) and the fact that O_{2i} preferentially accommodated in the vicinity of a B_s atom because the tetrahedral covalent radius of B_s atoms is 25% smaller than that of Si host atom [18, 20].

In 2006, Bothe and Schmidt found two different BO related recombination centers, the fast recombination center (FRC) occurring in the beginning few minutes of LID and the slow recombination center (SRC) as a major LID defect emerging after FRC [35]. The FRC and SRC are also considered fast and slow stages of LID degradation [43, 71]. Bothe and Schmidt reported defect generation energy $E_{gen.fast}=(0.23\pm0.02)\ eV$ for FRC and $E_{gen.slow}=(0.475\pm0.0235)\ eV$ for SRC. They also conveyed the defect annihilation energy $E_{ann.fast.1}=(0.32\pm0.02)\ eV$ and $E_{ann.fast.2}=(1.36\pm0.08)\ eV$ for FRC, as well as $E_{ann,slow}=(1.32\pm0.05)\ eV$ for SRC [35].

In 2010, Voronkov and Falster proposed the B_iO_2 model as LID defect since the B_s-O_{2i} complex could not explain the lifetime at the slow stage which, depended on the concentration of holes rather than boron concentration in the p-type material co-doped with boron and phosphorus. They explained that $(B_sO_2)^-$ as a latent complex existed already before illumination while $(B_sO_2)^+$ as a recombination active configuration proceed under LID [72]. However, they demonstrated the latent $(B_iO_2)^+$ complex as the major SRC, involving an interstitial atom B_i instead of B_s [72]. While emitted by oxygen precipitates, the self-interstitials penetrated into the bulk to produce the first B_i and then the B_iO_2 defect.

In 2016, Voronkov and Falster claimed the latent BO_2 defects at FRC and SRC stages were created during a cooling stage after high-temperature anneal as defect concentration depended on cooling rate and were proportional to the boron concentration and square oxygen concentration [71]. In contrast, Hallam et al. presented a single defect associated with fast and slow degradation caused by two traps level within the bandgap: acceptor and donor levels [73].

CHAPTER 3: MITIGATION OF LID

3.1 Introduction

Since BO complex was identified as the cause of LID in p-type B-doped Cz silicon, solar research have been conducted on how to minimize LID. This chapter will look into three main possibilities of avoiding LID including: (i) minimization/elimination (Chap. 3.2) (ii) recovery (Chap. 3.3) and (iii) regeneration (Chap. 3.4).

3.2 Minimization/ Elimination

As LID occurs in p-type B-doped Cz silicon with high BO complex concentration, several studies have been carried out on how to minimize or eliminate the LID. These include the following: (1) increasing the base resistivity ρ_{base} (Ω-cm) of p-type silicon substrate, (2) replacing p-type wafers with n-type wafers, (3) reducing the oxygen concentration by improving the silicon wafer fabrication, and (4) using alternative dopant rather than boron for silicon wafers. Table 3.1 summarizes the options and references on how to go about LID minimization and/or elimination

Table 3.1: Analysis of LID Minimization/Elimination.

year	High ρ_{base} (Ω-cm) (p-type B-doped)	n-type	Low Oxygen	No Boron
1997	1.0-10 [16]	P-doped Cz [16]		Ga-doped Cz [16]
1998		P-doped FZ [17]	FZ [17]	
1999	0.64 - 4.80 [21]		MCz [23]	
2000	0.13- 1.39 [22]			
2001	0.4 -11.6 [24]			
2004	1.0-14.0 [25]			Al- or In-doped Cz [25]
2009				P-doped Cz [26]

3.2.1. High Base Resistivity

The p-type boron-doped Cz silicon wafers with higher base resistivity ρ_{base} (Ω-cm) have been exploited for their better bulk carrier lifetime (τ_b *or* τ_{bulk}) [17, 27, 55], which demonstrates the Auger, Radiation, and SRH recombination influence (Eq. 3.1) [33]. The low boron concentration of the high ρ_{base} p-type substrates possibly contributes to the lower defect concentration and higher carrier lifetime if the BO complex is the trap causing LID. As shown in Fig. 3.1, under illumination, the *1.0 Ω-cm* resistivity wafer degraded more than the 10 Ω-cm counterpart, which displayed almost stable bulk carrier lifetime (τ_b) [28]. However, the high base-resistivity silicon wafers show lower efficiency because of the lower open circuit voltage and fill factor despite of the higher short circuit current.

$$\frac{1}{\tau_{bulk}} = \frac{1}{\tau_{Auger}} + \frac{1}{\tau_{Rad}} + \frac{1}{\tau_{SRH}} \qquad \text{(Eq. 3.1)}$$

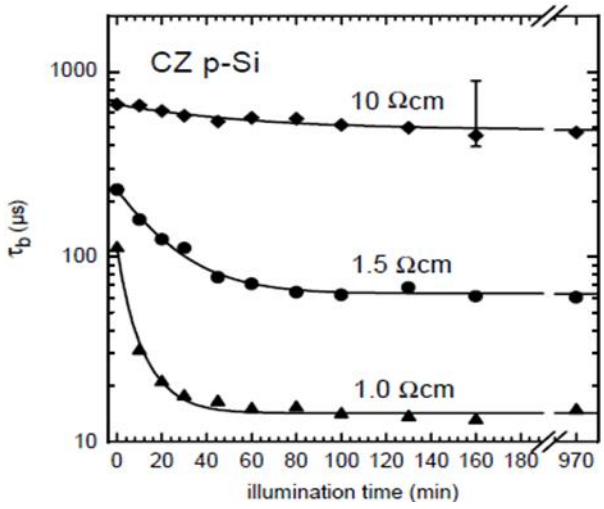

Fig 3.1: Measured τ_b degradation of boron-doped Cz Si wafers during illumination with halogen lamp (intensity 350 mW/cm^2=0.35 suns). Prior to the illumination, the wafers were annealed at 350°C for 10 min [28].

3.2.2. n-type Substrate

The use of the n-type wafers with phosphorous (P) [17, 33] or arsenic (As) [30] can also minimize/eliminate LID. In Fig 3.2, under illumination, the injected photons did not affect the bulk lifetime in n-type phosphor-doped Cz-Si wafers [16, 61]. However, for n-type solar cells, a slight LID influence could be observed due to the p-type B-doped layer making p-n junction in a solar cell [16, 47].

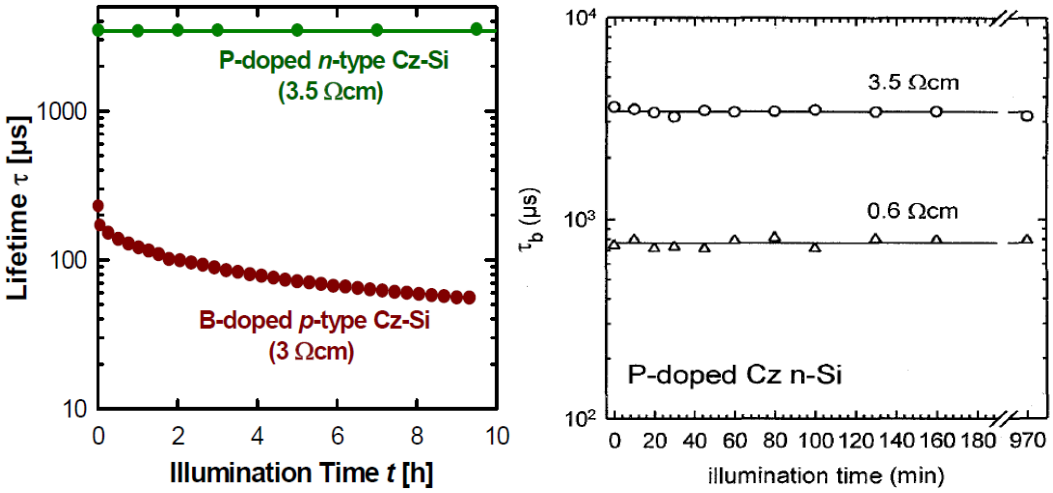

Fig 3.2 (Left): Measured lifetime of a boron-doped p- vs a phosphorus-doped n-type Cz-Si wafer as a function of illumination time (halogen lamp, 1 sun) [61].

(Right): Measured τ_b of phosphorus-doped (Phosphor-doped) Cz Si with two different resistivities (0.6 and 3.5 Ω-cm) during halogen lamp illumination (350 mW/cm^2=0.35 suns) [16].

3.2.3. Lower Oxygen Concentration

Low oxygen concentration in the silicon substrate can reduce the LID. For example magnetically-controlled environment has been used to produce the Cz silicon known as MCz with low oxygen [21, 32]. However, the Float Zone (FZ) [17, 21], is manufactured in an environment that inhibits the incorporation of oxygen into the boule and hence the very low oxygen content. Under the carrier injection ($\Delta n_a > 10^{13}$ cm^{-3}), the Cz Si wafer decayed severely compared to FZ and MCz silicon wafers (Fig 3.3: left) [56]. Under illumination, FZ silicon wafers with insignificant oxygen showed higher relative lifetime than Cz silicon although with the similar initial lifetime (Fig 3.3: right) [17]. Additionally, pure FZ-silicon with unmeasurable oxygen demonstrated stable relative lifetime under illumination, showing LID impact (Fig. 3.3: right) [17]. However, the pure silicon wafer manufacture costs expensive prices, increasing the budget.

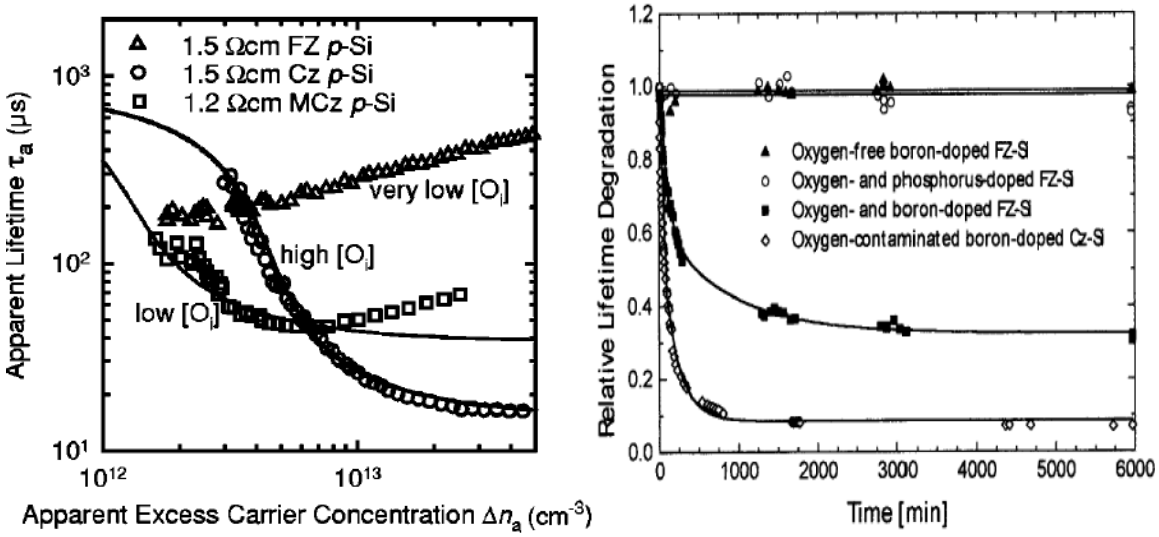

Fig 3.3 (Left): Measured apparent lifetime τ_a as a function of the apparent excess carrier concentration (Δn) (symbols) for three silicon materials with different interstitial oxygen concentrations. [O_i] = 57.53×10^{17} cm^{-3} for the high-O_i material, [O_i] = 56.53×10^{16} cm^{-3} for the low-O_i sample, and [Oi] = 53×10^{15} cm^{-3} for the very low O_i sample [56].

(Right): Lifetime degradation by 0.5 mΩ/cm2 while light verse time. Boron, phosphorus, and oxygen doped Fz as well as B-doped Cz Si samples exposed to carrier injection [17].

3.2.4. Alternative Dopants for p-type Substrate

Other group III dopants such as gallium (Ga) [16, 21, 24, 32], alumina (Al) [25], and Indium (In) [25, 54] have shown no LID. As illustrated in Fig 3.4 [21], the B-doped wafers degraded under irradiation; however, the Ga-doped wafers having low resistivity (*0.42* Ω-*cm*) displayed a stable effective lifetime (τ_{eff}), which represents the surface and bulk recombination (Eq. 3.2) [58]. Although LID can be avoided by applying alternative dopants for p-type wafers, the resistivity varies across the entire bulk due to low segregation coefficients. Moreover, the wafers from these alternative dopants are expensive because of low manufacturing volume.

$$\frac{1}{\tau_{eff}} = \frac{1}{\tau_{bulk}} + \frac{S_{front}}{W} + \frac{S_{back}}{W} \qquad \text{(Eq. 3.2)}$$

$$\frac{1}{\tau_{eff}} = \frac{1}{\tau_{bulk}} + \frac{J_{0\,front}(N_{dop} + \Delta n)}{qn_i^2 W} + \frac{J_{0back}(N_{dop} + \Delta n)}{qn_i^2 W} \qquad \text{(Eq. 3.3)}$$

where S is surface recombination velocity, W is the sample thickness, J_o is the saturation current density for characterizing the front and back surfaces recombination. N_{dop} is the back ground dopant density and n_i is the intrinsic carrier concentration in silicon.

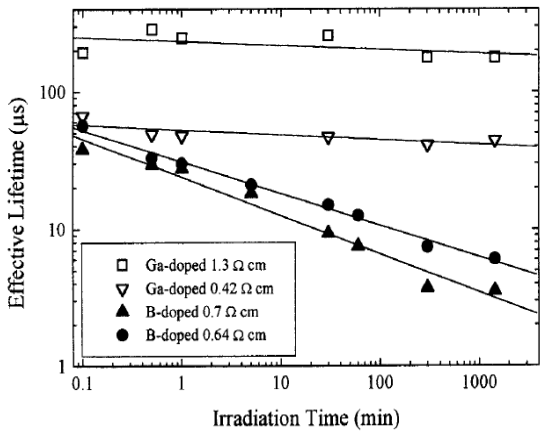

Fig 3.4: Comparison between B- doped and Ga-doped of low-resistivity Cz wafers for the relation between the effective lifetime versus AM 1.5 irradiation time [21].

3.3 Recovery

In 1973, Fisher and Pschunder observed LID as well as degradation/recovery cycle by low-temperature annealing at 80-200 °C for 1 hour [7]. Since then, the annealing of different temperatures [65] and time [33, 35, 36] has studied for recovery process. Table 3.2 summarizes the recovery treatments from various research.

Table 3.2: Annealing methods for the recovery from LID.

Condition	Low Temperature Annealing	RTP [68] Annealing/Firing
Temperature	180-450°C [65]	630-850°C [40]
Light/Dark	Dark	Infrared lamp
Time	10-30 min [38]	< 1 min

3.3.1 Low Temperature Anneal

Through the 200 °C annealing in the dark for 30 minutes, the low-injection bulk lifetime recovered from the LID decay (Fig. 3.5) [33]. It should be emphasized that both of the surfaces in the wafers were passivated with Si;Nx films deposited by remote plasma-enhanced chemical vapor deposition system (Oxford Plasma Technology) [33].

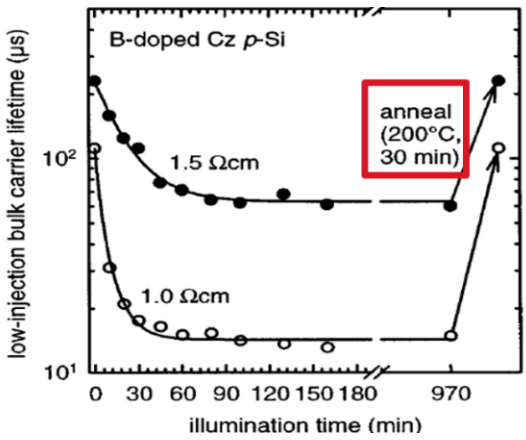

Fig 3.5: Measured changes of the low-injection bulk carrier lifetime (symbols) of two boron-doped Cz Si wafers with different resistivity under illumination with a halogen lamp (intensity 350 mW/cm^2) and during annealing in the dark at 200 °C for 30 min [33].

3.3.2 Rapid Thermal Processing (RTP) Anneal

Compared to the conventional furnace, the Rapid thermal processing (RTP) features lower budget and shorter time in PV production lines for (i) p-n junction formation (ii) contact annealing and (iii) forming gas anneal (FGA) [64]. In RTP chamber, a desired region of a sample can be heated because of burst of energy from infrared (IR) lamps. In the RTP IR belt furnace, the fast ramp up contributes to the uniform BSF formation [63] while the fast ramp down benefits the contact firing for low contact resistance [64]. For the LID analysis, the RTP short dwell time favors the effective hydrogenation of the bulk material [64]. Fig 3.6 shows that the effective lifetime recovered from LID after RTP belt furnace annealing (Table 3.3) [34].

Table 3.3: RTP temperature anneal treatment [34].

Condition	Experimental Set-up
Peak Temperature	760°C
Belt Speed	310 inch per min (ipm)
Light/Dark	Infrared lamp
Time	< 1 min for the whole process < 3 sec for the peak temperature

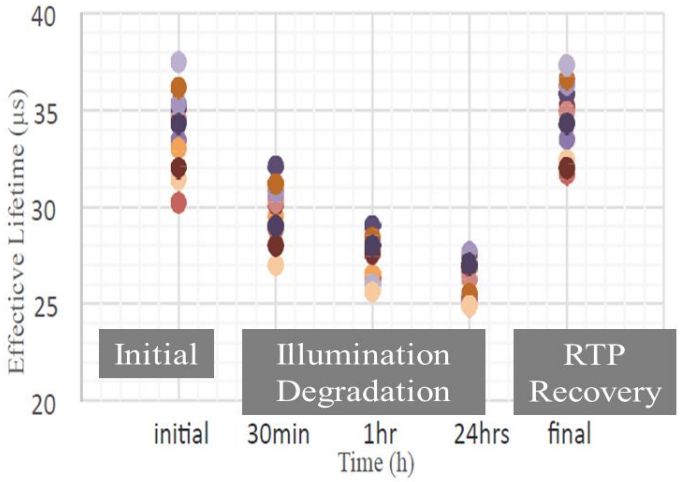

Fig 3.6: Effective lifetime measurements for different Cz-Si solar cells after 24-hour LID and final anneal process [34].

3.4 Regeneration

Even though annealing treatments have been observed to recover cells from LID through defect annihilation mechanisms [20, 35], the output performance of the recovered cells are still unstable when they are under illumination again [38, 43]. This situation motivates researchers to study reliable treatments for a stable recovery, which is called regeneration.

In 2006, Herguth et al. first proposed a new approach to permanently preventing the LID impact on B-doped Cz silicon solar cells by controlling the temperatures and carrier injection [44]. In this method, the cells were first annealed at 200°C on a hot plate in the dark for 30 min before starting the degradation experiment [44, 45]. In regeneration, the carrier injection was regulated by 0.5 V forward voltage or halogen lamp with light intensity of 1 sun while temperatures were controlled between 60-230°C, naturally heated by carrier injection or illumination (Table 3.4) [45]. Since then, some research groups have involved in similar regeneration procedures but varied the temperature range as shown in Table 3.4 [41, 44, 45, 47]. In this work, the similar concept was adopted to prove the regeneration as discussed in Chapter 4 and Chapter 5.

Table 3.4: Regeneration Treatments.

year	Research Group		Carrier Injection	Temperature
2006	Herguth et al. [44, 45]	1	1 sun	60-230°C
		2	0.5 forward voltage	60-230°C
2008	Lim et al. [41]		0.7 suns	135-165°C
2010	Lim et al. [47]		0.1 suns	70-220°C

Regarding the regeneration of Herguth et al. in 2006, the cells were first annealed at ~200°C in the dark for 30 min directly before LID and regeneration process. The cells degraded under 25°C illumination and recovered after regeneration at 60-230°C (Fig 3.7). Then, the regenerated cells were annealed at ~200°C again in the dark for 10-30 min [48]. For the stabilization test, the regenerated cells were exposed to 1 sun illumination at 25°C. Finally, the regenerated cells showed stabilization as illustrated in Fig. 3.8 [44, 45].

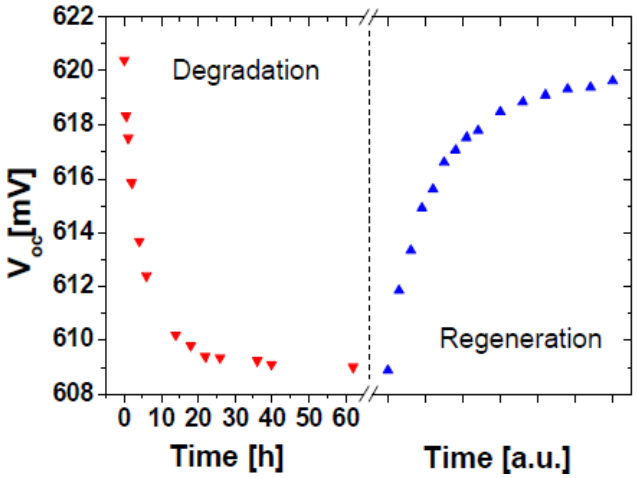

Fig 3.7: Degradation and subsequent regeneration cycle. The long time limit of regeneration probably equals the annealed state at the beginning of degradation [44].

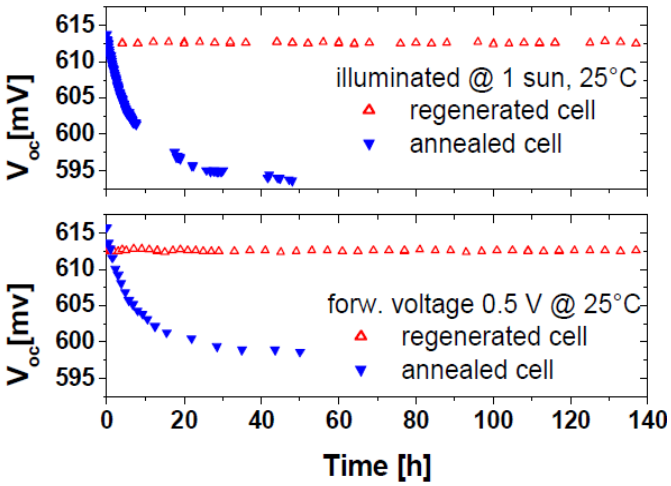

Fig 3.8: Stability test of a regenerated cell compared to a completely annealed cell. Degradation was induced by illumination (top) and applied forward voltage (bottom) [44].

CHAPTER 4: EXPERIMENTAL

4.1 Sample Preparation, Experimental Set-up and Measurement

This research work used the p-type B-doped Cz mono c-Si full Al-BSF solar cell with 90Ω/sq sheet resistance, $POCl_3$ diffused emitter, 2 Ω-cm base resistivity and 73 nm SiN_x:H antireflection coating (ARC) layer fabricated by plasma-enhanced chemical vapor deposition (PECVD). The sample cells were screen-printed with Ag gridlines on the front and full Al on the back as contacts. After the screen printing, RTP annealing was conducted for the contact formation (metallization) and p^+ BSF in Cz silicon by infrared (IR) belt furnace at ~774°C peak temperature at 300 inches per minute (ipm) belt speed.

For the experimental set-up, halogen lamps of 500W at 120V were used for illumination (Fig 4.1 left). The light intensity was detected by advanced Solar Survey 200R Irradiation Meter from SEAWARD (Fig.4.1: middle). The temperature of the solar cells was monitored by Infrared Thermometer from RYOBI (Fig. 4.1: right).

Fig 4.1: 500W and 120V halogen lamps for illumination (left). Infrared Thermometer (laser radiation) from RYOBI for temperature monitor (middle). Solar Survey 200R Irradiation Meter from SEAWARD for irradiation detection (right).

For the measurement, electrical output parameters (V_{oc}, I_{sc}, FF, and efficiency) were measured by I-V tester (Sinton Instruments FCT-350) as shown in Fig 4.2. The minority carrier lifetime was averaged with three measured values of three points in each cell by Suns-Voc (Sinton Instruments WCT-120) as shown in Fig 4.3.

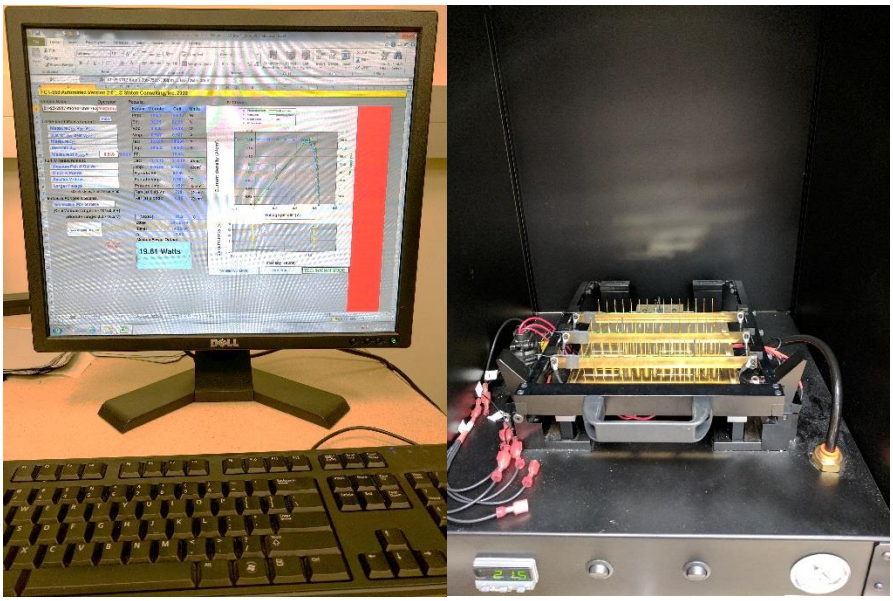

Fig 4.2: I-V tester, Sinton Instruments FCT-350) for the electronic outputs measurement.

Fig 4.3: Suns-Voc (Sinton Instruments WCT-120) for the effective lifetime measurement.

4.2 Experimental Design

In this work, experimental SET 1 and SET 2 were carried out (Fig 4.4, Fig 4.5). In SET 1, after screen printing and subsequent RTP contact co-firing, the freshly produced cells were exposed to 1 sun illumination at 70-100 °C for 120 hours - regeneration. For stabilization test, the regenerated cells were reserved in the dark at 22 °C for 20 days and then checked at 35-40°C under 0.1 suns illumination for 216 hours.

In SET 2, the freshly produced cells were first degraded at 35-40°C for 120 hours, and subsequently reserved at 22 °C in the dark for 77 days. The degraded cells were regenerated at 70-100°C under 1 sun illumination. Later, the regenerated cells were stabilized at 35-40°C under 0.1 suns for 72 hours.

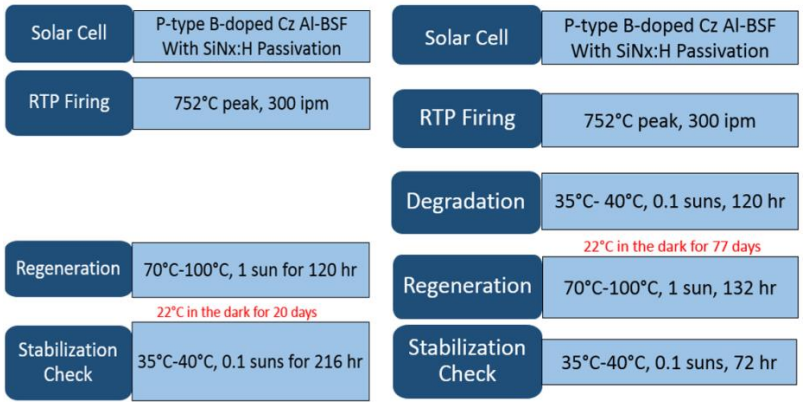

Fig 4.4: Experimental designs for SET 1 (left) and SET 2 (right).

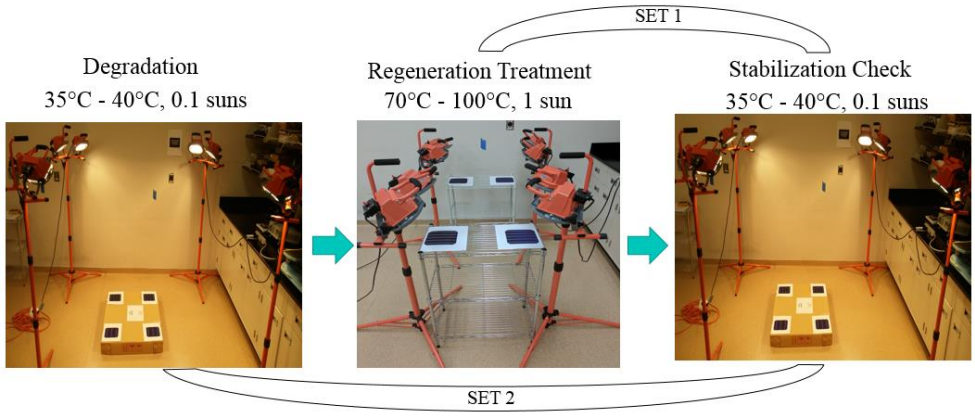

Fig 4.5: Illustration of experimental set-ups for SET 1 and SET 2.

CHAPTER 5: RESULTS AND DISCUSSIONS

The results of SET 1 (Fig 5.1) and SET 2 (Fig 5.2) showed that the cells were regenerated and stabilized successfully. However, as indicated by red circles in Fig 5.1 and Fig 5.2, the V_{oc} dropped down at the beginning of SET-1 regeneration due to LID rather than SET-2 regeneration. For SET 1, during the early period of regeneration, the B-H bonding and BO complex formation were competing under 1.0 sun illumination at 70-100°C. For SET 2, after the first degradation process, the degraded cells under regeneration, did not show the gap observed in SET 1, suggesting LID ineffectiveness in the SET-2 regeneration. Therefore, there was a gap in SER-1 regeneration but SET-2.

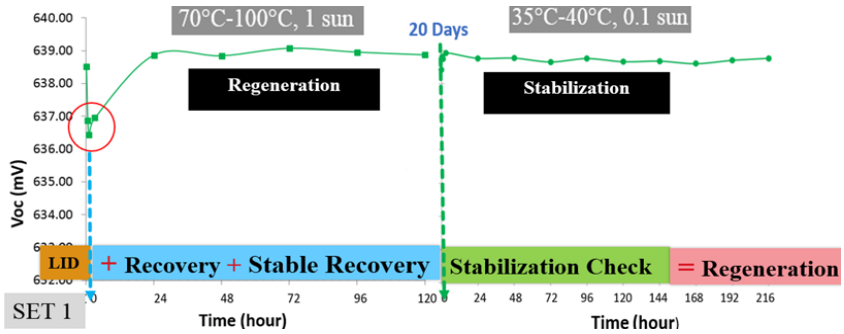

Fig 5.1: In SET 1, fresh cells showed a stable recovery under illumination (70-100°C) and no degradation in stabilization (35-40°C).

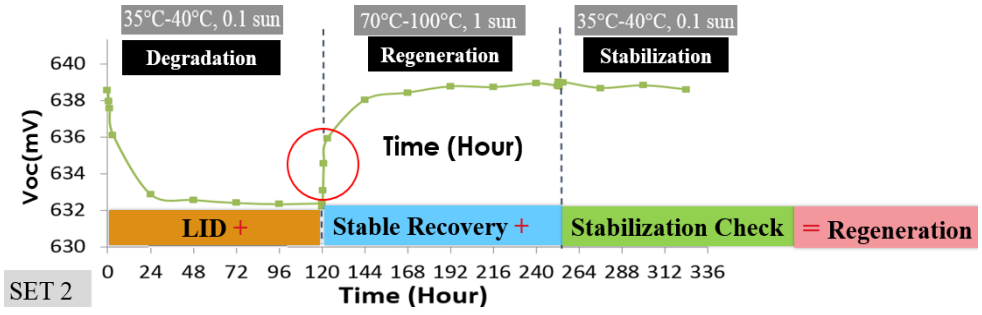

Fig 5.2: In SET 2, fresh cells first degraded under illumination at 35-40°C but subsequently recovered (70-100°C) and stabilized (35-40°C).

In the regeneration process under 1.0 sun illumination at 70-100°C, the photon injection stimulated hydrogen and defect into the excited state. Successively, the atomic hydrogen with mobility diffused and passivate the BO complex defect with the proper thermal energy temperature at 70-100°C (in this work). The passivated defect, possibly in the form of B-H, were in equilibrium after the complete reaction of atomic hydrogen and BO complex defect with sufficient time in regeneration. Therefore, the regenerated cells showed no degradation under illumination at low temperatures (35-40°C) − stabilization. Based on the results shown in Fig 5.1 and Fig 5.2., this work concludes that the whole regeneration process includes the simultaneous degradation, stable recovery, and stabilization

It should be emphasized that, before the regeneration treatment, the RTP co-firing after screen-printing assists the future atomic hydrogen passivated defects during regeneration process. The RTP short dwell time could result in hydrogen diffusion from the ARC layer with SiN_x:H into the bulk. According to Wilking et al [40], PECVD solar cells without firing do not recover from LID in regeneration. The RTP contact co-firing in this work plays the same role as the annealing pretreatment (before regeneration treatment) conducted by Herguth et al. [45] and Lim et al [47]. Moreover, before the stabilization test, this work did not conduct any annealing; however, Wilking et al. annealed the regenerated cells at ~200^{o}C on hotplate in the dark before they finally received stabilized results [48].

5.1 Hydrogenation for Recovery and Regeneration

The hypothesis behind the annealing recovery from LID is the hydrogenation. With the thermal energy in a specific temperature range of 60−400˚C [38, 70, 74], the hydrogen is able to diffuse in the bulk and the BO complex in the p-type base dissociates; meanwhile, boron might bind hydrogen together (B-H pairs) [38, 74].

However, the passivated defect are at non-equilibrium states in recovered cells annealed at ~200°C in the dark for 10-30 min. McQuaid et al. declared that atomic hydrogen is either highly mobile or highly unstable at quite low temperature about 200°C even though the ~200°C annealing in the dark for 30 min is sufficient to drive hydrogen into B-H or D-H (Defect-H) pairs [74]. Additionally, they demonstrated that B-H or D-H pairs is difficult to attach beyond 400°C for 30 minute [74].

This non-equilibrium passivated defect reverses to degradation under illumination possibly due to the lack of the sufficient excited energy generated by carrier injection from photons or forward bias. The carrier injection activates atomic hydrogen with intermolecular hydrogen bond at the electronic excited states [75]. This excited-state hydrogen bond (as B-H in this case) was shifted to lower energy levels, suggesting that the carrier injection benefits the passivated defect at a more stable state by controlling the Fermi-level shifting in regeneration process [75, 76]. This work concluded that both elevated temperatures (65-400°C) and carrier injection (> 0.1 suns) in regeneration enable the atomic hydrogen to passivate the defect in equilibrium − hydrogenation. The hydrogenation can be accelerated by properly increasing temperatures in low-temperature annealing [38], the intensity of the carrier injection [67], peak temperatures [40, 66] and belt speeds [39] in RTP co-firing.

In order to prove the hydrogenation principle, K.A. Münzer investigated the influence of hydrogen in silicon nitride of ARC layers on regeneration by comparing solar cells coated with PECVD (plasma-enhanced chemical vapor deposition) and LPCVD (low pressure chemical-vapor deposition) [42, 49]. Under the very similar regeneration condition of this work, his result demonstrated that only PECVD cells stably recovered rather than LPCVD cells (Fig. 5.3). Table 5.1 indicated that the main difference of PECVD and LPCVD is the hydrogen involvement during the fabrication, indirectly proving that hydrogen plays a key role in the regeneration process [49, 77]

Table 5.1: Comparison between PECVD and LPCVD [49].

	PECVD	LPCVD
Hydrogen	SiN_x:H	SiN_x
Regeneration	yes	no

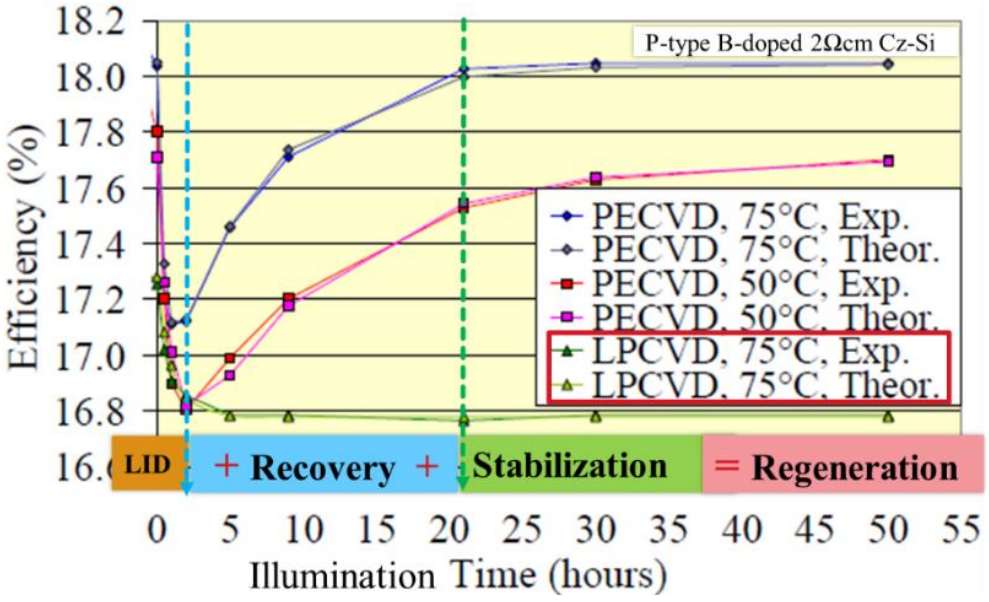

Fig 5.3: Efficiency degradation and regeneration of p-type solar cells with PECVD silicon nitride [49].

5.2 Three State Model versus New Proposed Three State Model

Three-state model has been used to explain the degradation, recovery and regeneration as discussed in Chapter 3. Based on the same concept, three schemes of the three-state model has been demonstrated by Herguth et al, Wilking et al, and Hallam et al.

Three-state model was first proposed by Herguth et al in 2006 [44] but kept changed until 2010 [50]. In the 2010 model (Fig 5.4), State A at a non-equilibrium status represents the inactive defect through annealing mechanisms. State B at a non-equilibrium condition exhibits the active defect suffering from LID or CID. State C is at an equilibrium stage demonstrates inactive defect after regeneration. Between State A and State B, the unstable defect can either degrade or recover mainly based on the temperatures. From State B to State A, the cells can regenerate from degradation. However, re-degradation from State C to State B or destabilization from State C to State B has not been observed because the inactive defect is at equilibrium State C. Also, the inactive defect at State A does not stabilize to State C but State A.

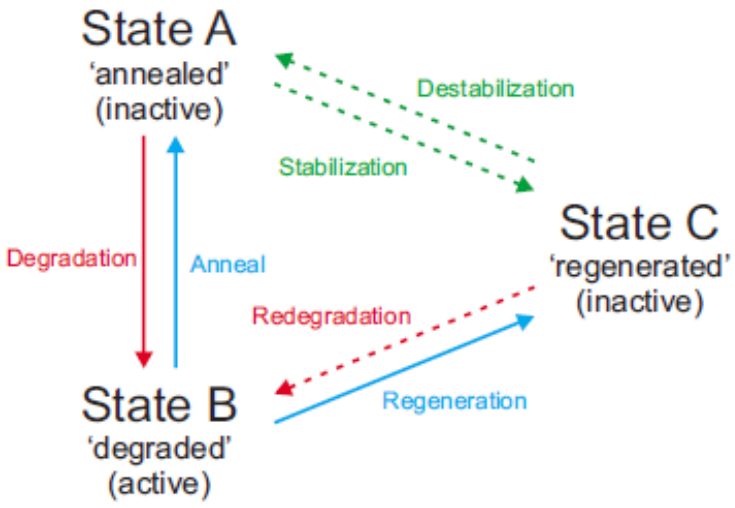

Fig 5.4: Working model of a three-state reaction scheme describing the boron-oxygen complex. Continuous arrows denote observed reactions, dashed reaction paths could not be verified so far [50].

In 2013, Wilking et al. [38, 39, 48] presented a similar three state model with the one from Herguth et al although they used “annealed state” to represent unstable “State A”, “degraded state” to stand for unstable “Sate B”, and “regenerated state” to show stable “State C”, as demonstrated in Fig 5.5 [38].

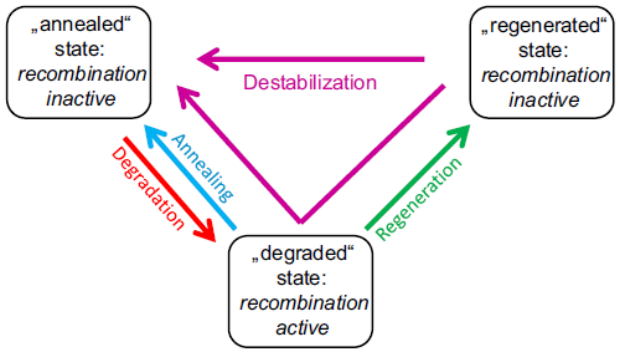

Fig 5.5: Transition reactions between the three BO related defect states. The transitions are activated under different temperature and illumination conditions, allowing their experimental separation. As a rule of thumb, annealing dominates at T>100°C in the dark, degradation at T<100°C under illumination, regeneration at 100°C<T<230°C under illumination in hydrogenated samples, and destabilization dominates at T>230°C [38].

Based on the previous models and hydrogenation, Hallam et al. proposed a basic three-state mathematical model [52, 53]. In their model, the defect dissociation inactivates recombination at State A, the defect formation activates recombination at State B, and the hydrogenated defect inactivates recombination at State C (Fig 5.6) [53].

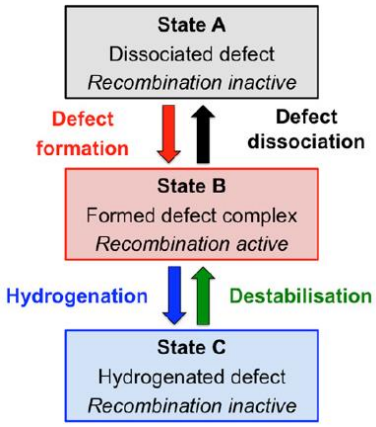

Fig 5.6: Diagrammatic representation for the three-state B-O defect system associated with CID in boron-doped Cz silicon [53].

A new three-state model is proposed in this work (Fig 5.7) while combining the idea of preceding three-state models. For unstable State A, the inactivated BO complex defect exists in both for the freshly cells after co-firing and the recovered counterparts through annealing. Nevertheless, Wilking et al. asserted that annealed state (State A) is activated only by purely thermal reaction since they used low temperature annealing in the dark [38]. However, in this work, the freshly screen-printed cells were metallized by RTP belt furnace, including carrier-injection and thermal activations.

At unstable State B, the BO complex defect is formed in a degraded solar cell due to LID. At stable State C, the BO complex defect is permanently passivated through hydrogenation in a regenerated cell. However, State D is declared by Herguth et al. in 2009 [51] without explaining why their regenerated cells destabilized [44]. State D is also included in this model although it was not observed experimentally in this work.

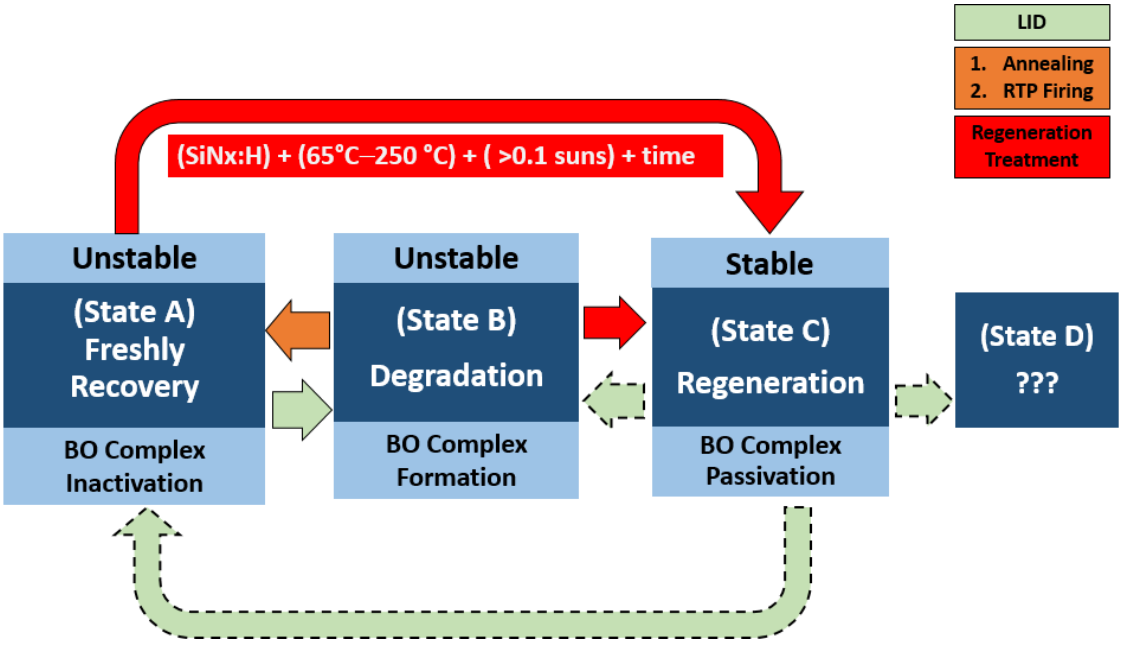

Fig 5.7: New proposed three-state model in this work; dash reaction paths have not observe in this research. Regeneration requires SiN_x:H in ARC [49,77], 65-400°C heating, >0.1 suns carrier injection [25], and sufficient time for whole hydrogenation process in equilibrium.

5.3. Onset Time of Recovery and Stabilization in Regeneration

In the comparison of the recovery onset time in regeneration, the effective lifetime started to recover after ~50 minutes at 70-100°C in this research (Fig 5.8: left) but after ~10 minutes at 140°C in Herguth et al. work [50] (Fig 5.8: right).

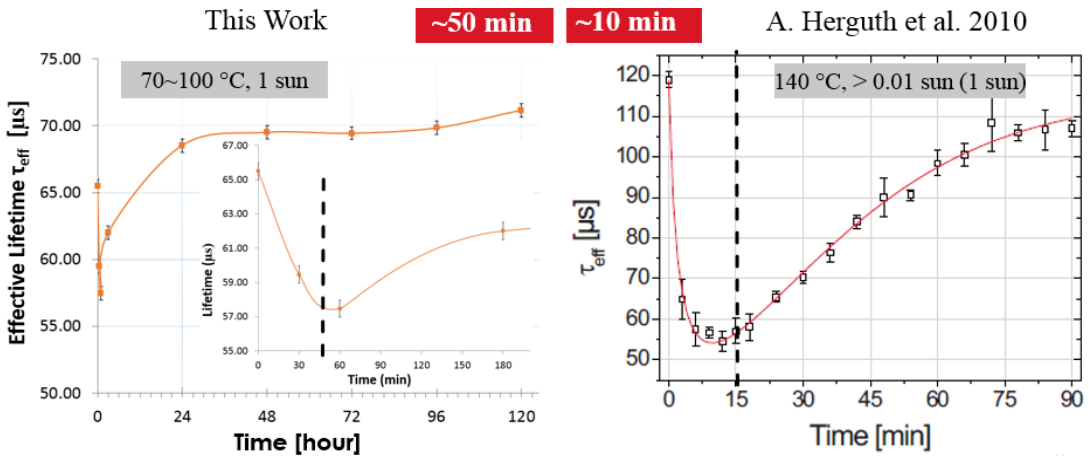

Fig 5.8: Onset time comparison of the recovery in regeneration between this work and the research of Herguth et al. [50].

In the comparison of the stabilization onset time in regeneration, the lifetime began to stabilize after 24 hours at 70-100°C in this work (Fig 5.9: left) compared to 20 hours at 165°C demonstrated by Lim et al (Fig 5.9: right) [46].

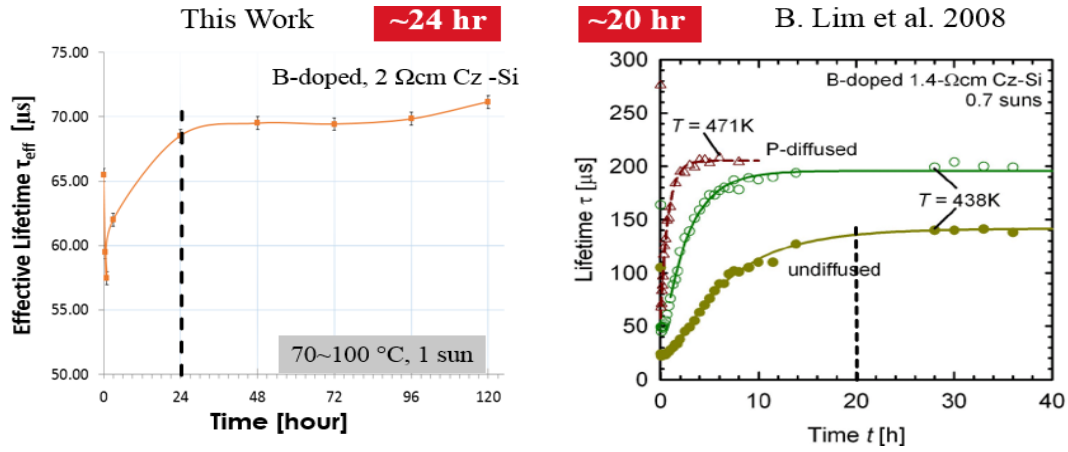

Fig 5.9: Onset time comparison of regeneration stabilization between this work and the research of Lim et al. [46]. (Left): Lifetime τ of Cz-Si samples with only B-doped (closed circles: P undiffused) and two P-diffused (open symbols) [46].

The defect stabilizes after 24 hours either in regeneration (Fig 5.10: left – this work) or degradation (Fig 5.10: right – Unsur et al [34]). This phenomenon could be explained with the defect property while the defect needs the similar time to be filled with excess carriers by carrier injection or hydrogenation through regeneration.

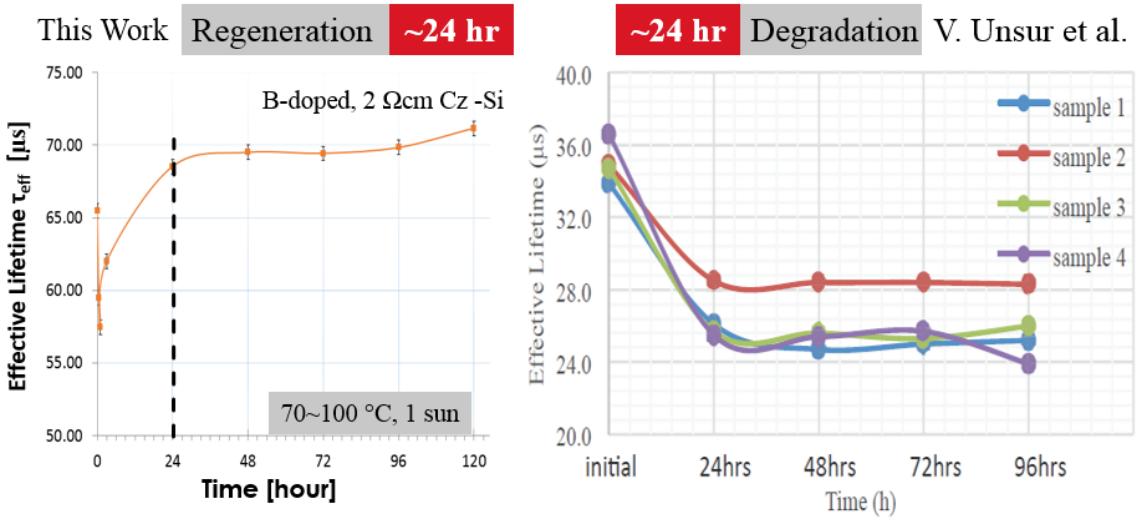

Fig 5.10: Onset time comparison of stabilization between the regeneration in this work and the degradation in the research of Unsur et al. [34].

5.4 Influence of Temperature on Regeneration Rate

Considering the aforementioned onset time of regeneration, the solar-cell samples, preparation/pretreatment and regeneration are analyzed in Table 5.2 [50, 46]. In analysis of Table 5.2 and Fig 5.11, this work concludes that the regeneration rates or time onsets are significantly influenced by regeneration temperatures in the range of 65-400°C.

Table 5.2: Analysis of the regeneration in p-type B-doped Cz Si solar cells.

		This Research	A. Herguth et al. [50]	B. Lim et al. [46]
contact		screen printing	screen printing	?
$POCl_3$ diffused emitter		90 Ω/sq	50 Ω/sq	100 Ω/sq
ARC layer		PECVD SiN_x:H	PECVD SiN_x:H	PECVD SiN_x:H
Annealing or Freshly		RTP 774°C, 300ipm for co-firing after screen printing	200°C annealing dark, 10 min for pretreatment	200°C annealing dark, 10 min for pretreatment
Treatment	Carrier Injection	1 sun	> 0.01 suns (1 sun)	> 0.7 suns
	Temperature	70-100 °C	140 °C	165°C
	Started Time	~50 min	~10 min	?
	Stable Time	~24 hr	?	~20hr

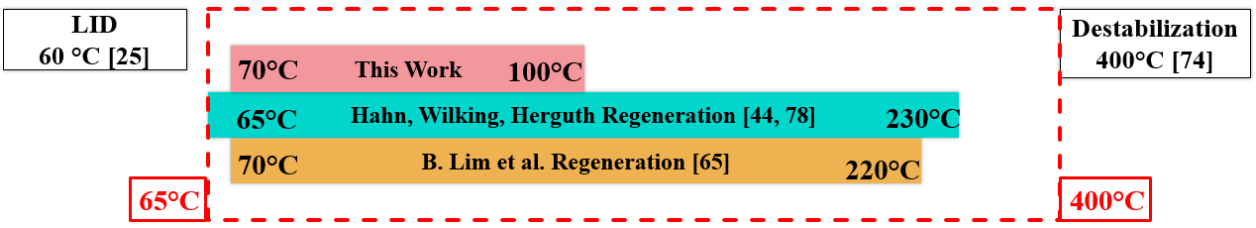

Fig 5.11: Analysis of the temperature impact on degradation, regeneration, and destabilization.

It should be noted that the sufficient carrier injection is necessary to facilitate the regeneration; otherwise, the cells cannot be regenerated despite heated in the regeneration temperature range. According to Schmidt et al [18, 25], the defect generation rate stabilizes when the light intensity is higher than 0.1 sun. In other words, the activation energy of the irradiation > 0.1 suns does not influence defect generation; however, it enables to function regeneration within 65-400℃ on the basis of the preceding hydrogenation discussion in Chap. 5.1. The similar correlation between regeneration rates and temperatures was also mentioned by Herguth et al., but they claimed that the regeneration operated at > 0.01 suns illumination at proper temperatures [50].

CHAPTER 6: CONCLUSION AND FUTURE SCOPE

6.1 Conclusion

Stable efficiency is a necessity for solar cell electricity to be adopted in every day power production. With p-type B-doped Cz mono c-Si Al-BSF solar cells, this work evaluated the causes, mitigations/elimination, and regeneration of LID. The regeneration process was investigated with two experimental set-ups – LID before regeneration and regeneration without first degrading. The regeneration experiments were controlled with the carrier injection (~1 sun), temperatures (70-100°C) and sufficient time.

For regeneration to occur, the presence of the hydrogen in the silicon bulk is necessary. In screen-printed cells, hydrogen is able to diffuse from the ARC layer (SiN_x:H) into the bulk through the RTP metallization co-firing. The regeneration process requires (i) carrier injection of > 0.1 suns (ii) elevated temperatures ranging of 65-400°C, and (iii) the sufficient time for hydrogen to completely passivate the defect into an equilibrium status. These influences on regeneration should operate simultaneously and obligatorily.

The whole regeneration process encompasses the first degradation, subsequent recovery and final stabilization. The regeneration rate is significantly impacted by temperatures – higher temperature within the proper range obviously accelerates the regeneration.

6.2 Future Scope

First future topic is the regeneration acceleration by controlling light intensity and temperatures. For light intensity, higher irradiation, such as laser [67, 69], assists regeneration rate. For temperature, it could be included (i) low-temperature annealing in pretreatments or RTP co-firing after screen printing, and (ii) regeneration temperatures.

Second, it is supportive to compare Al-BSF p-type B-doped Cz silicon solar cells to other p-type B-doped Cz cells with various structures, such as multi-crystalline, compensated p-type B-doped, and passivated emitter contact (PERC) solar cells.

Last but not least, it is crucial to find the kinetic model by evaluating the impact of thermal activation energy on (i) the FRC and SRC stages, (ii) single defect or two defects, (iii) the whole regeneration process, including LID, recovery, and stabilization.

REFERENCES

[1] Edmond Becquerel, “Mémoire sur les effets électriques produits sous l'influence des rayons solaires,” Comptes Rendus. No.9: p561–p567 (1839)

[2] Wikipedia, “Timeline of solar cells,” May 2017
View Online: https://en.wikipedia.org/wiki/Timeline_of_solar_cells

[3] Arthouros Zervos (Chairman of REN21), “Global Overview” in Renewables 2016- Global Status Report, REN 21 Renewable Energy Policy Network for the 21st Century, Paris, France, ISBN 978-3-9818107-0-7, ch. 1, pp29, pp41 (2016)
View Online: http://www.ren21.net/status-of-renewables/global-status-report/

[4] Nian Chen, “Understanding and development of cost-effective industrial Aluminum Back Surface Field (Al-BSF) silicon solar cells,” Ph.D dissertation, Dept. Electron. Eng., Univ. NC Charlotte, NC (2015)

[5] Chris Meehan, “Solar PV Production May Break 50 Gigawatt Barrier in 2014” Clean Energy Authority.com: Solar Energy News, November 2013
View Online: http://www.cleanenergyauthority.com/solar-energy-news/solar-production-50-gw-in-2014-110613/

[6] Energysaga, “Mono vs. Poly solar panels explained,” energysaga, May, 2017
View Online: https://www.energysage.com/solar/101/monocrystalline-vs-polycrystalline-solar-panels/

[7] H. Fischer and W. Pschunder, "Investigation of photon and thermal induced changes in silicon solar cells," in Photovoltaic Specialists Conference, 10 th, Palo Alto, Calif, pp. 404-411, (1974)

[8] V. G. Weizer, H. W. Brandhorst, J. D. Broder, R. E. Hart, and J. H. Lamneck, "Photon-degradation effects in terrestrial silicon solar cells”, Journal of Applied Physics 50, 4443 (1979); doi: 10.1063/1.326437,
View online: http://dx.doi.org/10.1063/1.326437

[9] S.W. Glunz, S. Rein, W. Warta, J. Knobloch, and W. Wettling, “On the degradation of Cz-silicon solar cells”, Presented at the 2nd World Conference on Photovoltaic Solar Energy Conversion, Vienna, 1998, pp.1343-1346

[10] W. Shockley and W. T. Read, Jr., “Statistics of the Recombinations of Holes and Electrons,” Phys. Rev. 87, pp835, September 1952

[11] R. N. Hall, “Electron-Hole Recombination in Germanium” Phys. Rev. 87, pp387, July 1952

[12] R.L. Crabb, “Photon Induced Degradation of Electron and Proton Irradiated Silicon Solar Cells,” 9th IEEE Photovoltaic Specialist Conference, vol. 20, no. 6, pp243-249, Dec. 1973; DOI: 10.1109/TNS.1973.4327402

[13] Christiana Honsberg and Stuart Bowden, “Type of Recombination”, PV Education ORG, ch. 3.3 (May, 2017)
View Online: http://pveducation.org/pvcdrom/types-of-recombination

[14] Jan Schmidt and Andre´s Cuevas, "Electronic properties of light-induced recombination centers in boron-doped Czochralski silicon," JOURNAL OF APPLIED PHYSICS, Vol. 86, No. 6, pp3175-3180, September 1999; DOI: 10.1063/1.371186

[15] S. Rein and S. W. Glunz, "Electronic properties of the metastable defect in boron-doped Czochralski silicon:Ðnambiguous determination by advanced lifetime spectroscopy," Appl. Phys. Lett. 82, 1054 (2003); doi: 10.1063/1.1544431

[16] J. Schmidt, A.G. Aberle, and R. Hezel, "INVESTIGATION OF CARRIER LIFETIME INSTABILITIES IN CZ-GROWN SILICON," 26th IEEE PVSC, Anaheim, CA, 1997, p. 13.

[17] S.W. Glunz, S. Rein, W. Warta, J. Knobloch, and W. Wettling, "ON THE DEGRADATION OF CZ-SILICON SOLAR CELLS," Presented at the 2nd World Conference on Photovoltaic Solar Energy Conversion, Vienna, 1998, pp.1343-1346

[18] J. Schmidt, K. Bothe, and R. Hezel, "FORMATION AND ANNIHILATION OF THE METASTABLE DEFECTEN BORON-DOPED CZOCHRALSKI SILICON," Proceedings of the 29th IEEE, Photovoltaic Specialists Conference, New Orleans, LA, USA, pp178-181 (2002); DOI: 10.1109/PVSC.2002.1190485

[19] Jan Schmidt and Rudolf Hezel, "LIGHT-INDUCED DEGRADATION IN CZ SILICON SOLAR CELLS: UNDAMENTAL UNDERSTANDING AND STRATEGIES FOR ITS AVOIDANCE," 12th Workshop on Crystalline Silicon Solar Cell Materials and Processes, Breckenridge, Colorado, August 2002, pp1-8

[20] M. Ametowobla, G. Bilger, J. R. Köhler, and J. H. Werner, “Laser induced lifetime degradation in p-type crystalline silicon,” Journal of Applied Physics, 111, 114515 (2012); doi: 10.1063/1.4725191;
View online: http://dx.doi.org/10.1063/1.4725191

[21] Tadashi Saitoh, Hiroshi Hashigami, Stefan Rein, and Stefan Glunz, "Overview of Light Degradation Research on Crystalline Silicon Solar Cells," Pro. Photovolt. Res. Appl. 2000, 8: pp537-547

[22] Jan Schmidt and Andrés Cuevas, “PROGRESS IN UNDERSTANDING AND REDUCING THE LIGHT DEGRADATION OF CZ SILICON SOLAR CELLS,” Presented at the 16th EU PVSEC, Glasgow, May 2000

[23] Jianhua Zhao, Aihua Wang and Martin A. Green "24.5% effciency Silicon PERT Cells on MCZ Substrates and 24.7% Efficiency PERL Cells on FZ Substrates," Prog. Photovolt: Res. Appl. No.7, pp471-474 (1999)

[24] S.W. Glunz, S. Rein, W. Warta, J. Knobloch, W. Wettling,"Degradation of carrier lifetime in Cz silicon solar cells" Solar Energy Materials & Solar Cells, No. 65, pp219-229(2001)

[25] J. Schmidt, "Structure and transformation of the metastable boron- and oxygen-related defect center in crystalline silicon," PHYSICAL REVIEW B, 69, 024107 (2004); DOI: 10.1103/PhysRevB.69.024107

[26] D. Macdonald, A. Liu, F. Rougieux1 A. Cuevas, B. Lim2 J. Schmidt, M. Di Sabatino and L. J. Geerligs, "BORON-OXYGEN DEFECTS IN COMPENSATED P-TYPE CZOCHRALSKI SILICON," 24th EU PVSEC, Hamburg, Germany, pp877-882, Sep. 2009

[27] Jan Schmidt and Armin G. Aberle, "Accurate method for the determination of bulk minority-carrier lifetimes of mono- and Multicrystalline silicon wafers," Journal of Applied Physics, 81, 6186 (1997); doi: 10.1063/1.364403; View online: http://dx.doi.org/10.1063/1.364403

[28] Jan Schmidt and Armin G. Aberle, "New Method For The Accurate Determination of Bulk Carrier Lifetimes of Crystalline Silicon Wafers For Solar Cells,"14TH EU PVSEC, Barcelona, Spain, pp2396-2399; June 1997

[29] J. Schmidt, A.G. Aberle, and R. Hezel, "Investigation Of Carrier Lifetime Instabilities on Cz-Grown Silicon," 26th IEEE PVSC, Anaheim, CA, 1997, p. 13

[30] Chengquan Xiao, Xuegong Yu, Deren Yang, Duanlin Que, “Study on permanent deactivation of the light-induced degradation in p-type compensated crystalline silicon solar cells” Solar Energy Material & Solar Cells, 117: 29-33 (2013)

[31] Donald A. Neamen, “Excess Carrier Lifetime: Shockley-Real-Hall Theory of Recombination” in Semiconductor Physics and Devices: Basic Principles, Fourth Edition, New York, US, McGrew-Hill, 2010, ch. 6.5, sec. 1, pp221-222

[32] Jan Schmidt, "Light-Induced Degradation in Crystalline Silicon Solar Cells" Solid State Phenomena, Vols. 95-96, pp. 187-196 (2004); DOI: 10.4028 View Online: http://www.scientific.ne

[33] Jan Schmidt, Christopher Berge, and Armin G. Aberle, "Injection level dependence of the defect-related carrier lifetime in light-degraded boron-doped Czochralski silicon", Applied Physics Letters, Volume 73, No.15: pp2167-2169 (1998); doi: 10.1063/1.122411

[34] Veysel Unsur, Babar Hussain and Aba Ebong, "Complete Recovery of Light Induced Degradation of Cz Silicon solar Cells with Rapid Thermal Processing," 43rd IEEE PVSC, June 2016; DOI: 10.1109/PVSC.2016.7749695

[35] Karsten Bothe and Jan Schmidt, "Electronically activated boron-oxygen-related recombination centers in crystalline Silicon" J. Appl. Phys. 99, 013701 (2006); doi: 10.1063/1.2140584; View online: http://dx.doi.org/10.1063/1.2140584

[36] Karsten Bothe, Ron Sinton and Jan Schmidt, "Fundamental Boron–Oxygen-related Carrier Lifetime limit in Mono- and Multicrystalline Silicon" Prog. Photovolt: Res. Appl; No.13, pp287–296, (2005); DOI: 10.1002/pip.586

[37] Jan Schmidt, Andres Cuevas, Stefan Rein, and Stefan W. Glunz, "Impact of Light Induced Recombination Centers on the Current-Voltage Characteristic of Czochralski Silicon Solar Cells," Prog. Photovol: Res. Appl., No. 9, p249-p255, (2001); DOI: 10.1002/pip.373

[38] Svenja Wilking, Cornelius Beckh, Sebastian Ebert, Axel Herguth, Giso Hahn, "Influence of bound hydrogen states on BO-regeneration kinetics and consequences for high-speed regeneration processes," Solar Energy Materials & Solar Cells, No.131, pp2–8 (2014)

[39] Svenja Wilking, Josh Engelhardt, Sebastian Ebert, Cornelius Beckh, Axel Herguth, Giso Hahn, "HIGH SPEED REGENERATION OF BO-DEFECTS: IMPROVING LONG-TERM SOLAR CELL PERFORMANCE WITHIN SECONDS", 29th EU PVSEC, pp366-372, (2014)

[40] Svenja Wilking, Sebastian Ebert, Axel Herguth, and Giso Hahn, "INFLUENCE OF SHORT HIGH TEMPERATURE STEPS ON THE REGENERATION OF BORON-OXYGEN RELATED DEFECTS," 28th European Photovoltaic Solar Energy Conference and Exhibition, pp34-38, (2013)

[41] Bianca Lim, Karsten Bothe, and Jan Schmidt, "Deactivation of the boron–oxygen recombination center in silicon by illumination at elevated temperature," phys. stat. sol. (RRL) 2, No. 3, pp93–95 (2008); DOI 10.1002/pssr.200802009

[42] K.A. Münzer, M.G. Winstel, A. Krause, R.E. Schlosser,"SOLAR CELL PROGRESS by PROCESS EVOLUTION", 3rd European Photovoltaic Solar Energy Conference and Exhibition, Valencia, Spain, p1875-p1878, (2008)

[43] Bianca Lim, Vladimir V. Voronkov, Robert Falster, Karsten Bothe, and Jan Schmidt, “Lifetime recovery in -type Czochralski silicon due to the reconfiguration of boron–oxygen complexes via a hole-emitting process”
Appl. Phys. Lett. 98, 162104 (2011); doi: 10.1063/1.3581215,
View online: http://dx.doi.org/10.1063/1.3581215

[44] Axel Herguth, Gunnar Schubert, Martin Kaes, Giso Hahn,“A new approach to prevent the negative impact of the metastable defect in boron doped Cz silicon solar cells,” 4th IEEE Photovolt. Waikoloa, HI, USA, pp940-943, (2006);
DOI: 10.1109/WCPEC.2006.279611

[45] A. Herguth, G. Schubert, M. Kaes and G. Hahn, "Investigations on the Long Time Behavior of the Metastable Boron–Oxygen Complex in Crystalline Silicon," Prog. Photovolt: Res. Appl. 2008; 16:135–140 (2008)

[46] Lim, Bianca, Sonja Hermann, Karsten Bothe, Jan Schmidt, and Rolf Brendel. "Permanent deactivation of the boron-oxygen recombination center in silicon solar cells." In Proceedings of the 23rd European Photovoltaic Solar Energy Conference, p. 1018. 2008.

[47] Bianca Lim, Fiacre Rougieux, Daniel Macdonald, Karsten Bothe, and Jan Schmidt, "Generation and annihilation of boron–oxygen-related recombination centers in compensated - and -type silicon," J. Appl. Phys. 108, 103722 (2010); doi: 10.1063/1.3511741; View online: http://dx.doi.org/10.1063/1.3511741

[48] S. Wilking, A. Herguth, and G. Hahn, "Influence of hydrogen on the regeneration of boron-oxygen related defects in crystalline silicon", Appl. Phys. 113, 194503 (2013); doi: 10.1063/1.4804310,
View online: http://dx.doi.org/10.1063/1.4804310

[49] K.A. Münzer, "HYDROGENATED SILICON NITRIDE FOR REGENERATION OF LIGHT INDUCED DEGRADATION"Ò4th European Photovoltaic Solar Energy Conference, p1558-p1561, (2009)

[50] Axel Herguth and Giso Hahn, "Kinetics of the boron-oxygen related defect in theory and experiment,"Đournal of Applied Physics 108, 114509 (2010);
doi: 10.1063/1.3517155

[51] Axel Herguth and Giso Hahn, "BORON-OXYGEN RELATED DEFECTS IN CZ-SILICON SOLAR CELLSÝEGRADATION, REGENERATION AND BEYOND" 24th EU PVSEC, Sep. 2009, Hamburg, Germany, p974-p976

[52] Brett Hallama, Malcolm Abbotta, Jose Bilbaoa, Phill Hamerb,a, Nicholas Gormana,Đoonyong Kima, Daniel Chena, Katherine Hammertona, David Paynea, Catherine Chana, Nitin Nampallia, Stuart Wenhama, "Modelling kinetics of the boron-oxygen defect system" 6th International Conference on Silicon Photovoltaics, SiliconPV 92 (2016) 42 – 51; doi: 10.1016/j.egypro.2016.07.008

[53] Brett Hallam, Malcolm Abbott, Nitin Nampalli, Phill Hamer, and Stuart Wenham, "Influence of the formation- and passivation rate of boron-oxygen defects for mitigating Carrier-induced degradation in silicon within a hydrogen-based model" J. Appl. Phys. 119, 065701 (2016); doi: 10.1063/1.4941387; View online: http://dx.doi.org/10.1063/1.4941387

[54] Eunhwan Cho, Young-Woo Ok, Ajay D. Upadhyaya, Martin Jeff Binns, Jesse Appel, Jason Gup, Member IEEE, and Ajeet Rohatgi, Fellow, IEEE, "P-type Indium-Doped Passivated Emitter Rear Solar Cells (PERC) on Czochralski Silicon Without Light-Induced Degradation" IEEE Journal of Photovoltaics, VOL.6, NO. 4: p795-p800 (2016)

[55] Franziska Wolny, Torsten Weber, Matthias Müller, Gerd Fischer, "Light Induced Degradation and Regeneration of High Efficiency Cz PERC Cells with Varying Base Resistivity" Silicon PV, 38: 523-530 (2013)

[56] Jan Schmidt, Karsten Bothe, and Rudolf Hezel, "Oxygen-related minority-carrier trapping centers in p-type Czochralski silicon",Appl. Phys. Lett. 80, 4395 (2002); doi: 10.1063/1.1483908, View online: http://dx.doi.org/10.1063/1.1483908

[57] R.A. Sinton and A. Cuevas, "A Quasi-Steady-State Open-Circuit Voltage Method For Solar Cell Charateriszation," 16th EU PVSEC 1-5, May 2000

[58] WCT-120, Photoconductance Lifetime Tester and Optional Suns-Voc User Manual, Sinton Instruments, v 3.0, Boulder, CO, USA, 2006-2013

[59] Karsten Bothe, Jan Schmidt, and Rudolf Hezel, "Comprehensive Analysis of The Impact of Boron and Oxygen on The Metastable Defect in Cz Silicon" 3rd World Conference on Photovoltaic Energy Conversion, 4P-A8-68, 2003

[60] Mohamed M. Hilali, Kenta Nakayashiki, Abasifreke Ebong and Ajeet Rohatgi, "High-efficiency (19%) Screen-printed Texured Cells on Low-resistivity Float-zone Silicon with High Sheet-resistance Emitters" Progress In Photovoltaics Research and Applications, 2006; 14:135-144, DOI:10.1002/pip.688

[61] J. Schmidt, K.Bothe, R. Bock, C. Schmiga, R. Krain, R. Brendel, "N-type Silicon- The Better Material Choice For Industrial High-Efficiency Solar Cells?" N-type European Photovoltaic Solar Energy Conference, p998-p1001, (2007)

[62] Phillip Hamer, Brett Hallam, Malcolm Abbott, and Stuart Wenham, "Acceleration formation of the boron-oxygen complex in p-type Czochralski siliocn" Phys. Status Solidi RRL 9, No. 5: pp297-300 (2015), DOI: 10.1002/pssr.201510064

[63] A. Rohatgi, A. Ebong, V. Yelundur and A. Ristow, “Rapid Thermal Processing of Next Generation of Silicon Solar Cells” PROGRESS IN PHOTOVOLTAICS: RESEARCH AND APPLICATIONS, No 8: 515-527 (2000)

[64] A. Ebong, N. Chen, A. Chowdhury, and V. Unsur, “The impact of rapid thermal processing (RTP) in crystalline silicon solar cell performance and light induced degradation (LID)” 42nd IEEE PVSC, New Orleans, 2015

[65] Bianca Lim, Karsten Bothe, and Jan Schmidt, "Impact of oxygen on the permanent deactivation of boron–oxygen-related recombination centers in crystalline silicon," JOURNAL OF APPLIED PHYSICS 107, 123707 2010, DOI: 10.1063/1.3431359 · Source: IEEE Xplore

[66] D. Sperber, F. Furtwänler, A. Herguth, G. Hahn, “On Stability of Dielectric Passivation Layers Under Illumination and Temperature Treatment,” 32nd EU PVSEC, München, Germany, pp 523-526 (2016)

[67] Xi Wang, Mattias Juhl1, Malcolm Abbott, Ziv Hameiri, Yu Yao and Alison Lennon, “Use of QSSPC and QSSPL to monitor recombination processes in p-type silicon solar cells” 4th International Conference on Silicon Photovoltaics, SiliconPV, No. 55, pp.169 – 178 (2014)

[68] Dominic C. Walter, Bianca Lim1 and Jan Schmidt, “Realistic efficiency potential of next-generation industrial Czochralski-grown silicon solar cells after deactivation of the boron–oxygen-related defect center,” Prog. Photovolt: Res. Appl.; No.24, pp920–928 (2016); DOI: 10.1002/pip.2731

[69] Brett Hallam, Phillip Hamer, Nitin Nampalli, Malcolm Abbott, Moonyong Kim, Daniel Chen, Azmeer Azmi, Nicholas Gorman, Hongzhao (Alex) Li, Pei Hsuan (Doris) Lu, Sisi Wang, Alison Wenham, Catherine Chan, David Payne, Ly Mai, Jingjia Ji and Stuart Wenham, “RAPID PROCESSING OF BORON OXYGEN DEFECTS,” 31st EU PESEC, Hamburg, Germany, (2016); DOI: 10.4229/EUPVSEC20152015-2DO.16.4

[70] E A Davis, N Piggins and S C Bayliss, “Optical properties of amorphous SiN_x(:H) films” J. Phys. C: Solid State Phys. 20 (1987) 415-4427.

[71] Vladimir Voronkov, Robert Falster, “The nature of boron-oxygen lifetime-degrading centres in silicon” Current Topics in solid state physics, Volume 13, Issue 10-12, p712-p717 (2016), DOI: 10.1002/pssc.201600016

[72] V. V. Voronkov and R. Falster, Latent complexes of interstitial boron and oxygen dimers as a reason for degradation of silicon-based solar cells, Citation: Journal of Applied Physics 107, 053509 (2010); doi: 10.1063/1.3309869, View online: http://dx.doi.org/10.1063/1.3309869

[73] Brett Hallam, Malcolm Abbott , Tine Nærland, and Stuart Wenham, “Fast and slow lifetime degradation in boron-doped Czochralski silicon described by a single defect” P hys. Status Solidi RRL 10, No. 7, 520–524 (2016) / DOI 10.1002/pssr.201600096

[74] S. A. McQuaid, M. J. Binns, and R. C. NewmanE. C. LightowlersJ. B. Clegg, “Solubility of hydrogen in silicon at 1300 °C” Citation: Appl. Phys. Lett. 62, 1612 (1993); doi: 10.1063/1.108602, View online: http://dx.doi.org/10.1063/1.108602

[75] GUANG-JIU ZHAO AND KE-LI HAN, “Hydrogen Bonding in the Electronic Excited State” ACCOUNTS OF CHEMICAL RESEARCH ,Vol. 45, No. 3: p404–p413 (2012)

[76] Marcus Gläsera, Dominik Lausch. “Towards a quantitative model for BO regeneration by means of charge state control of hydrogen” Energy Procedia 77 (2015) 592 – 598

[77] N. Nampalli, B. Hallam, C. Chan, M. Abbott, and S. Wenham, "Evidence for the role of hydrogen in the stabilization of minority carrier lifetime in boron-doped Czochralski silicon," Applied Physics Letters 106, 173501 (2015); doi: 10.1063/1.4919385, View online: http://dx.doi.org/10.1063/1.4919385

[78] Giso Hahn, Svenja Wilking, Axel Herguth, “BO-related Defects: Overcoming Bulk Lifetime Degradation in crystalline Si by Regeneration” Erschienen in: Solid State Phenomena; NO. 242: p80-p89 (2016)